ENGINEERING RESEARCH INSTITUTE
THE UNIVERSITY OF MICHIGAN
ANN ARBOR

GENERAL DESIGN PROCEDURE FOR HIGH-EFFICIENCY TRAVELING-WAVE AMPLIFIERS

Technical Report No. 24
Part I

Electron Tube Laboratory
Department of Electrical Engineering

By

Joseph E. Rowe
Harold Sobol

Project 2750

CONTRACT NO. AF30(602)-1845
DEPARTMENT OF THE AIR FORCE
PROJECT NO. 4506, TASK NO. 45152
PLACED BY: THE ROME AIR DEVELOPMENT CENTER
GRIFFISS AIR FORCE BASE, NEW YORK

February, 1958

ABSTRACT

A general design procedure is developed for the design of both low-power and high-power high-efficiency traveling-wave amplifiers. The process is based on the selection of optimum values (for highest efficiency) of the design parameters C, QC, B and b from the large-signal curves and design of an amplifier with the particular type of r-f structure specified by power and bandwidth requirements and operating parameters as near the optimum values as possible. In cases where the optimum design parameters cannot all be realized simultaneously the design engineer will be able to select the parameter that he wishes to compromise.

The procedure is first developed for helix-type tubes and then correction factors are derived that permit the design of amplifiers with any type of r-f structure from the same set of curves.

EXPLANATORY NOTES

1. Theoretical Development of Design Procedure. In Part I of this report a general design procedure is developed for the design of high-efficiency traveling-wave amplifiers. The procedure is first developed for helix-type tubes and is then extended to cover traveling-wave amplifiers with other types of r-f structures. The same design curves are used for these dispersive structures with appropriate correction factors.

2. Design Curves. In Part II all of the available design curves useful in the actual design of high-efficiency amplifiers are compiled. Immediately preceding each section of curves there is a list of parameters for which the particular curves have been calculated.

TABLE OF CONTENTS

LIST OF FIGURES

LIST OF FIGURES
(Continued)

GENERAL DESIGN PROCEDURE FOR HIGH-EFFICIENCY TRAVELING-WAVE AMPLIFIERS

INTRODUCTION

Both low-power and high-power traveling-wave amplifiers are used in a variety of applications and high-power tubes in particular must frequently operate at as high an efficiency as possible. Hence a simple design procedure is much to be desired. Heretofore, high-power traveling-wave amplifiers have been designed using Pierce's small-signal theory and the design then modified according to previously obtained experimental results in order to achieve high saturation output and a reasonable efficiency. In this paper large-signal results[1,2,3] on the theoretical performance of traveling-wave amplifiers are used as the basis of a general design procedure to obtain near-maximum power output and efficiency at any frequency range. The large-signal curves are independent of frequency and apply to all forms of traveling-wave tubes presently in use, within the limitations noted in the developments. The chief limitation in the theory is that the electric field is assumed constant across the stream radius. This assumption is considered valid for values of the stream diameter parameter B up to 0.5 to 0.75 as indicated by experimental studies of traveling-wave tube efficiency reported by Cutler[4]. Other extensive experimental results on traveling-wave tube efficiency have been presented by Caldwell[5] for a wide range of operating conditions and attenuator configurations. If it is assumed that the electric field varies as $I_o(\gamma r)$ across the stream small-signal relationships can be used to predict that the efficiency will be reduced from the uniform field value by a factor 0.8 when B = 1. The true reduction factor is probably between 0.8 and 0.9.

The large-signal efficiency curves apply to tubes with all types of r-f structures; hence, to design a high-power amplifier of a particular structure, the multi-dimensional efficiency curves must be intersected with a surface determined by the impedance vs. $\gamma a'$ curve for the structure. The intersection of these two surfaces defines the maximum efficiency that can be achieved with the particular structure.

Helix-type tubes have the advantage of a relatively broad bandwidth of operation (2 to 1 in frequency) and have sufficient power-handling capabilities, subject to thermal limitations, for many applications. However, when very high power levels are needed the helix cannot be used and the designer must resort to other structures such as various forms of modified helices (loaded) or periodically loaded waveguides. These high-impedance structures unfortunately have inherently narrow bandwidths of operation compared with the helix.

The design procedure for the helix-type tube is based on evaluating the helix impedance from the usual reduction factors on the sheath-helix impedance. In the case of modified helix or periodically loaded waveguide structures, the structure impedance is also related to the sheath-helix impedance by appropriate factors.

In order to design a traveling-wave tube with the particular type of r-f structure specified by power and bandwidth requirements, optimum (for high efficiency) values of the design parameters C, QC, B and b are selected from the large-signal curves and the design adjusted to produce operating parameters as near the optimum values as possible.

LARGE-SIGNAL RESULTS

The large-signal curves have been computed assuming a ratio of helix-to-beam diameter a'/b' equal to 2; thus $\gamma a' = 2\gamma b'$ where $B = \gamma b'$. Values of

a'/b' between 1.4 and 2.0 are typical in experimental tubes, depending upon the type of focusing used and the means of suppression of backward-wave oscillations. Fortunately the large-signal curves are relatively independent of a'/b'.

A typical set of large-signal efficiency curves in which η_s is a function of QC and B is shown in Fig. 1 for C = 0.1. The value of the velocity parameter b has been optimized at each point to give maximum η_s. It is seen that for C = 0.1 the maximum saturation efficiency occurs for QC $\approx$ 0.125 and B $\approx$ 1.0. Extensive comparisons have been made between the above theoretical results and experimental results from several laboratories and reasonably good agreement has been found over a considerable range of the parameters. Tien[6] has also presented large-signal calculations on the traveling-wave amplifier based on a one-dimensional model.

DERIVATION OF HELIX DESIGN EQUATIONS

In order to develop a traveling-wave amplifier design procedure it is necessary to obtain an expression for the helix impedance as a function of frequency. The impedance of an actual helix mounted in its supporting structure is calculated by multiplying the sheath-helix impedance as calculated by Fletcher[7] by the appropriate reduction factors to account for wire size, wire spacing and dielectric loading. The impedance vs. $\gamma a'$ curves for a sheath helix of various a'/b' ratios are shown in Fig. 2[7]. The ordinates of the curves are related to the sheath-helix impedance by

$$K_s' = K_s \frac{\beta_o}{\gamma}\left(1 + \frac{\beta_o^2}{\gamma^2}\right)^{3/2}, \qquad (1)$$

where $\beta_o = \omega/c$,

$\gamma^2 = \beta^2 - \beta_o^2$, and

K_s = the sheath-helix impedance.

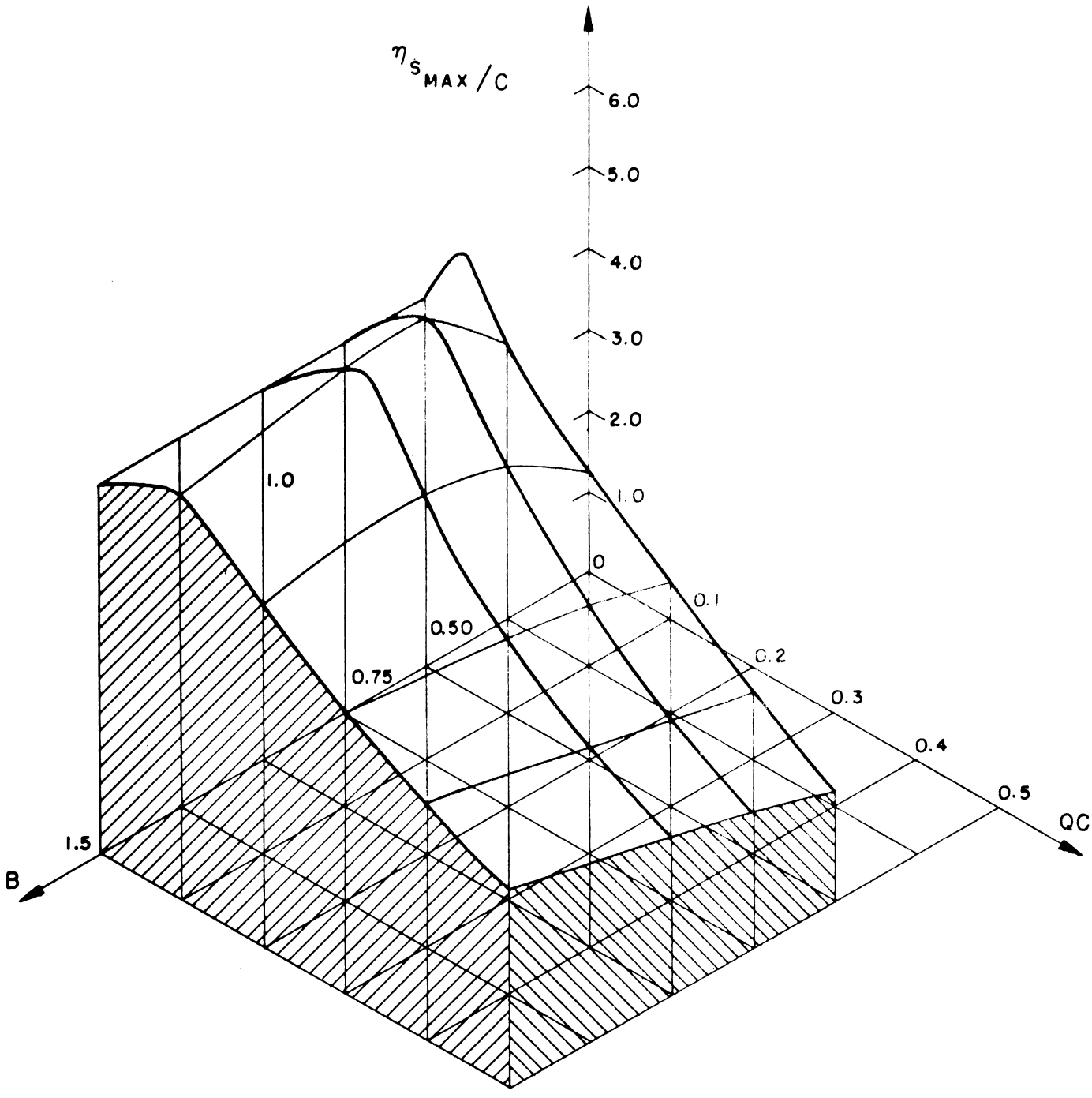

FIG. 1 MAXIMUM SATURATION EFFICIENCY /C VS. SPACE CHARGE AND BEAM DIAMETER.
($C = 0.1$, $d = 0$, $A_0 = 0.0225$, $a'/b' = 2.$)

FIG. 2

SHEATH-HELIX IMPEDANCE K_s FOR SOLID ELECTRON BEAM. HELIX-TO-BEAM RADIUS AS THE PARAMETER

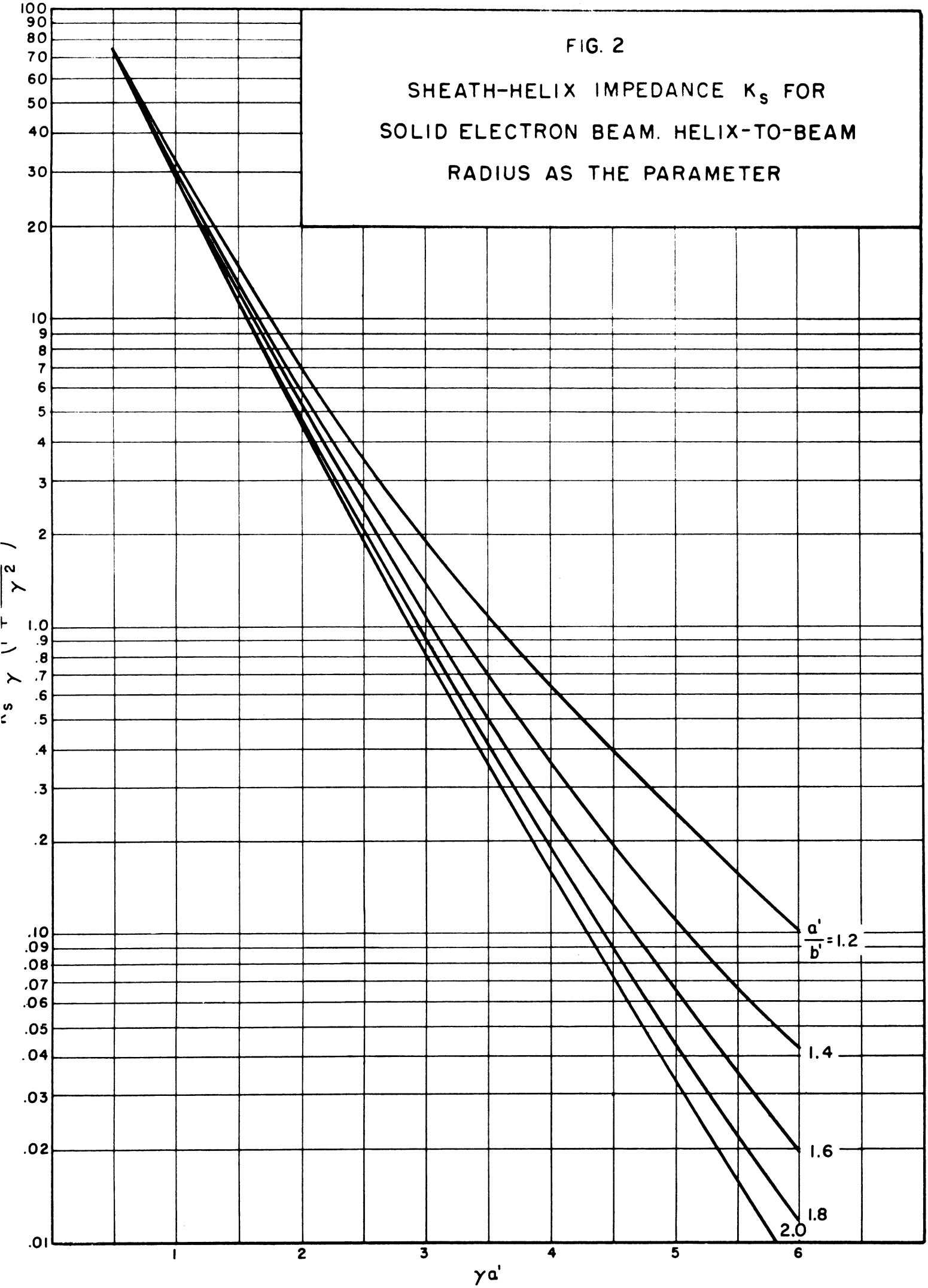

Since the helix retarded wavelength is usually small compared to λ_o, Eq. 1 may be written as

$$K_s' = K_s \frac{\beta_o}{\gamma} . \qquad (2)$$

The wave phase velocity may be approximated as $v = v_o(1+Cb)/(1-Cy)$, where $1 + Cb \approx 1 - Cy$; hence the sheath-helix impedance can be written as

$$K_s = \frac{506\ K_s'\ (1 + Cb)}{V_o^{1/2}} , \qquad (3)$$

where C = the gain parameter,

b = the velocity parameter,

V_o = the beam voltage, and

y = the phase constant of the r-f wave.

It is known experimentally that the impedance of an actual helix is always less than K_s, sometimes as small as $K_s/2$. In most instances a good approximation to the actual helix impedance may be found by multiplying the sheath-helix impedance K_s by the reduction factor F calculated by Tien[8]. Tien's reduction factors F_1 and F_2 are for a sheath to a tape helix and consider the effect of both dielectric loading and space harmonic fields. He has of course made some approximations and hence there is some restriction on the range of validity of his results. However, good agreement with experimental results has been found at many frequencies and for both wire and tape helices.

Tien presents the reduction factors as F vs. $\beta_o a'$ curves, but they may be plotted vs. $\gamma a'$ with voltage as the parameter in the following way.

The phase constant is written as

$$\beta_o a' = \frac{\beta_o}{\gamma} \gamma a' = \frac{v}{c} \gamma a' \ . \qquad (4)$$

Using the approximate expression for the wave phase velocity given before Eq. 3, we can write Eq. 4 as

$$\beta_o a' = \frac{1.977 \times 10^{-3} \ V_o^{1/2} \ \gamma a'(1 - Cy)}{1 + Cb} \ . \qquad (5)$$

Usually both Cy and Cb may be neglected in comparison with unity. Also, as pointed out earlier $(1-Cy)/(1+Cb) \approx 1$. Thus Eq. 5 may be simplified to

$$\beta_o a' = 1.977 \times 10^{-3} \cdot V_o^{1/2} \cdot \gamma a' \ . \qquad (6)$$

Tien's calculations of the helix-impedance reduction factors were not extensive enough to determine F vs. $\gamma a'$ curves over a wide range of helix voltages. The impedance reduction factor $F = F_1 \cdot F_2$ shown in Fig. 3 was calculated for a wide range of $k_i a$ and DLF from Tien's data using $\delta/p = 1/5$ and a value of F_2 assumed independent of $k_i a$. The data shown in these figures are then used to calculate curves of the helix-impedance reduction factor vs. $\gamma a'$ for particular values of beam voltage and dielectric loading factor. A typical plot of F vs. $\gamma a'$ is shown in Fig. 4 for a DLF of 90 percent.

Using the reduction factor F calculated above gives the actual helix impedance K as

$$K = F \ K_s = \frac{506 \ F \ K_s' \ (1 + Cb)}{V_o^{1/2}} \ . \qquad (7)$$

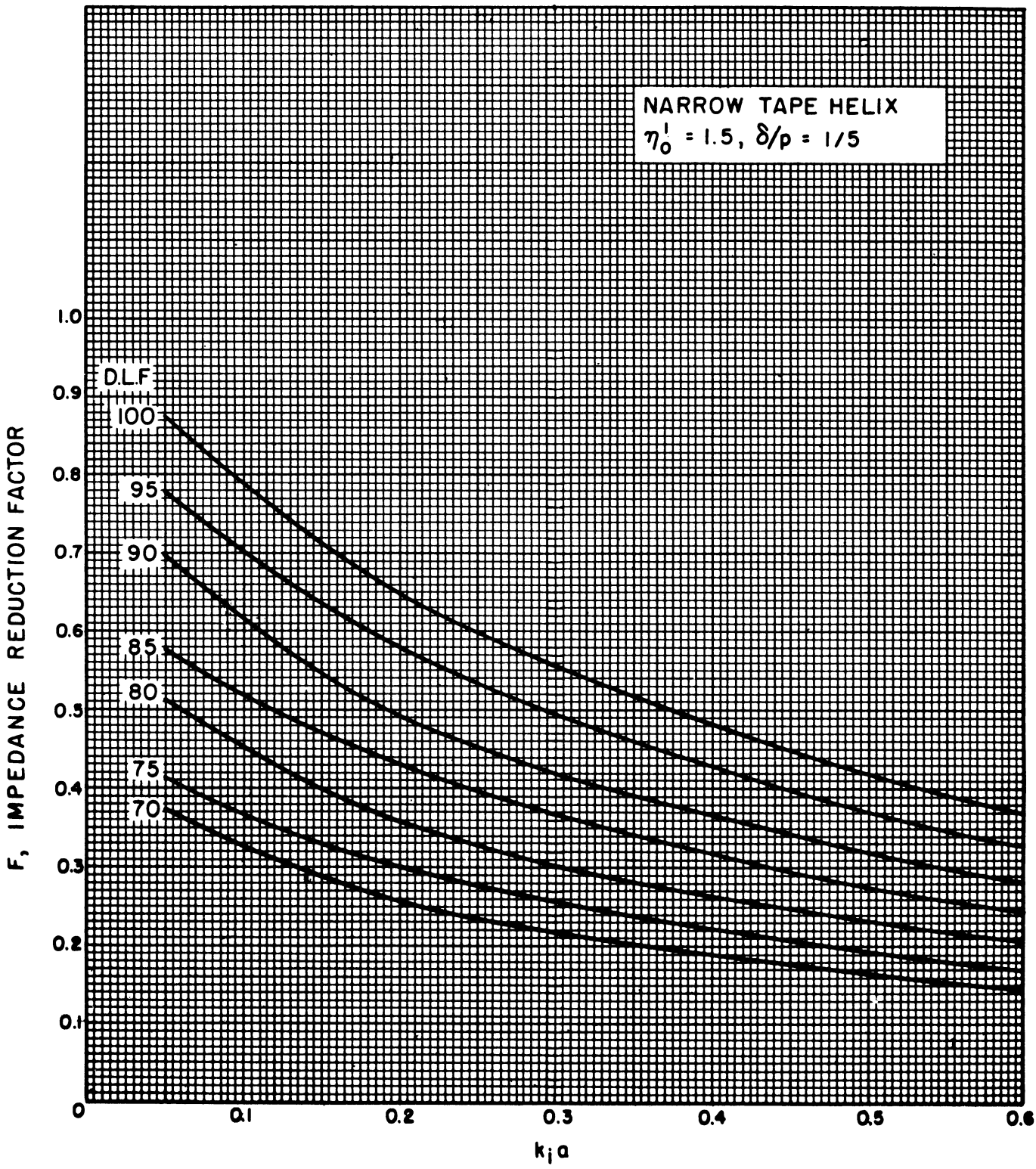

FIG. 3 IMPEDANCE REDUCTION FACTOR $F = F_1 F_2$ FOR A TAPE HELIX. (EXTENSION OF TIEN'S CALCULATIONS.)

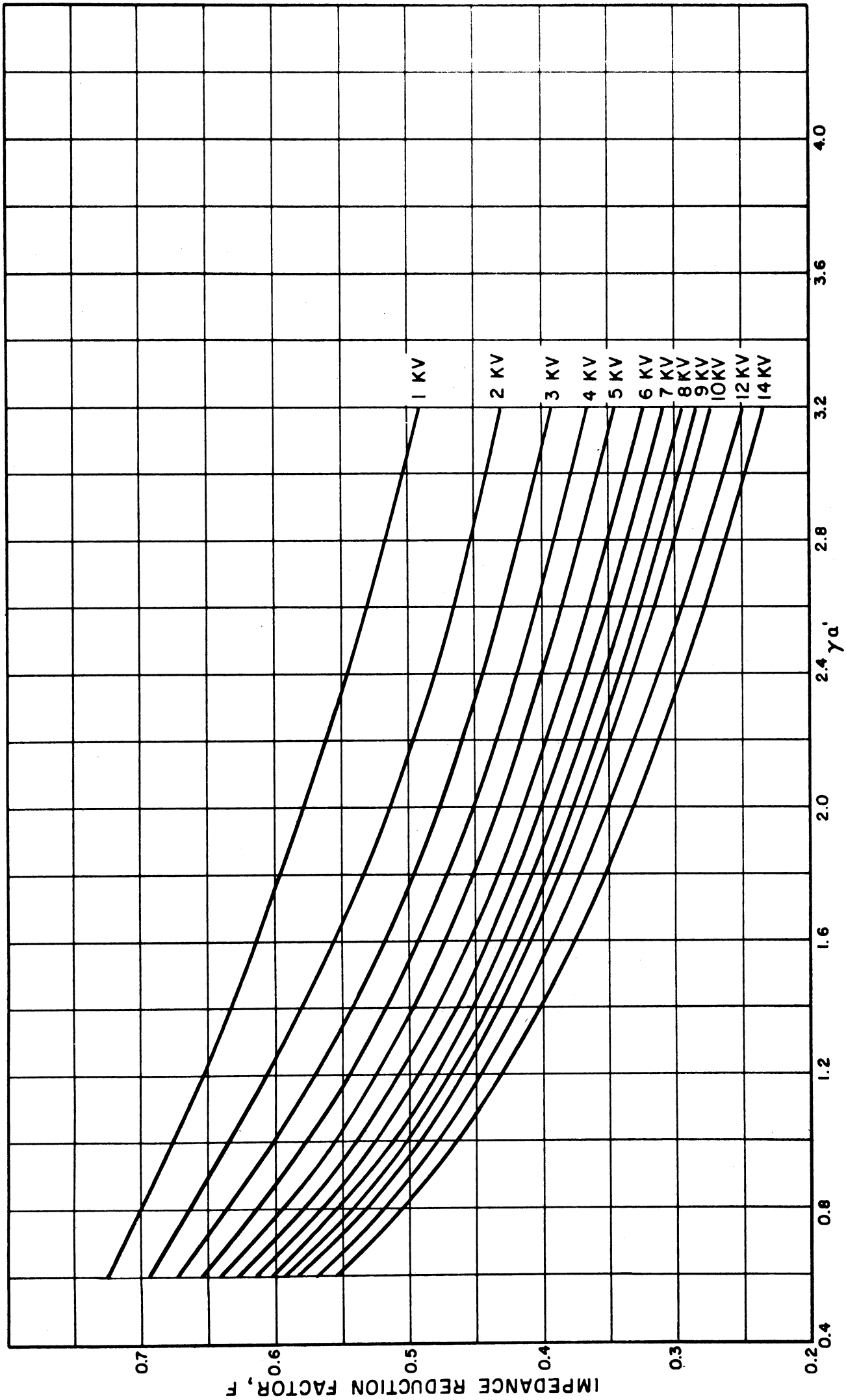

FIG. 4 HELIX IMPEDANCE REDUCTION FACTOR F FOR VARIOUS VALUES OF BEAM VOLTAGE.
(DLF = 90 %)

The traveling-wave-tube gain parameter may then be written as

$$C^3 = \frac{F\, K_s\, I_o}{4\, V_o} , \tag{8}$$

where I_o = the d-c stream current. Combining Eqs. 7 and 8 yields an expression for beam perveance in terms of the helix impedance and the gain parameter:

$$P_\mu = \frac{7905\, C^3}{F\, K_s'\, (1 + Cb)} , \tag{9}$$

where $P_\mu = \frac{I_o}{V_o^{3/2}} \cdot 10^6$, beam micropervs.

The small-signal space-charge parameter QC may be expressed in terms of the gain parameter and the radian plasma frequency as

$$QC = \frac{1}{4C^2} \left(\frac{\omega_q/\omega}{1 + \omega_q/\omega} \right)^2 , \tag{10}$$

where $\omega_q/\omega = (\omega_p/\omega)\, R_h$ = an effective normalized plasma frequency. The normalized plasma frequency is given by

$$\left(\frac{\omega_p}{\omega} \right)^2 = \frac{\eta\, I_o}{\pi \epsilon\, b'^2\, u_o \omega^2} , \tag{11}$$

where $\eta = e/m$, the charge-to-mass ratio for the electron, and the beam diameter or space-charge range parameter B is

$$B = \beta b' = \frac{\omega}{v}\, b' = \frac{\omega\, (1 - Cy)\, b'}{u_o} . \tag{12}$$

Then the normalized effective plasma frequency ω_q/ω may be written as

$$\left(\frac{\omega_p}{\omega}\right)^2 R_h^2 = \left(\frac{\omega_q}{\omega}\right)^2 = \frac{R_h^2 (1 - Cy)^2 P}{\pi\epsilon_o (2)^{3/2} \eta^{1/2} B^2} , \qquad (13)$$

where $P = I_o/V_o^{3/2}$, the beam perveance.

Equation 10 for the space-charge parameter thus becomes

$$QC = \frac{59.97}{\left[\frac{B}{R_h}\left(\frac{F\ Ks'}{C}\right)^{1/2} \frac{(1 + Cb)^{1/2}}{1 - Cy} + 15.48\ C\right]^2} . \qquad (14)$$

Again $1 + Cb \approx 1 - Cy$; also, the second term in the denominator of the above equation is usually small compared to the first. Hence Eq. 14 may be simplified to

$$QC \approx \frac{60\ (1 + Cb)}{\left[\frac{B}{R_h}\left(\frac{F\ Ks'}{C}\right)^{1/2} + 15.5\ C\right]^2} . \qquad (15)$$

A further simplification of Eq. 15 can be made by neglecting Cb compared to unity. This approximation is usually valid for values of C up to about 0.1. Figures 5 and 6 are typical graphs of Eq. 15, with ordinates of QC/(1+Cb). Each group assumes particular values of a'/b', V_o and dielectric loading.

Figure 7 is a plot of the optimum value of the electron velocity parameter b vs. QC both for maximum small-signal gain and for maximum saturation efficiency when B = 1, d = 0. The value of the injection velocity parameter that gives maximum small-signal gain is shown vs. x_1 for particular values of QC and C in Figs. 8 and 9. It is noticed that the effect of increasing the loss factor is to shift the entire set of curves to the left[9]. The value

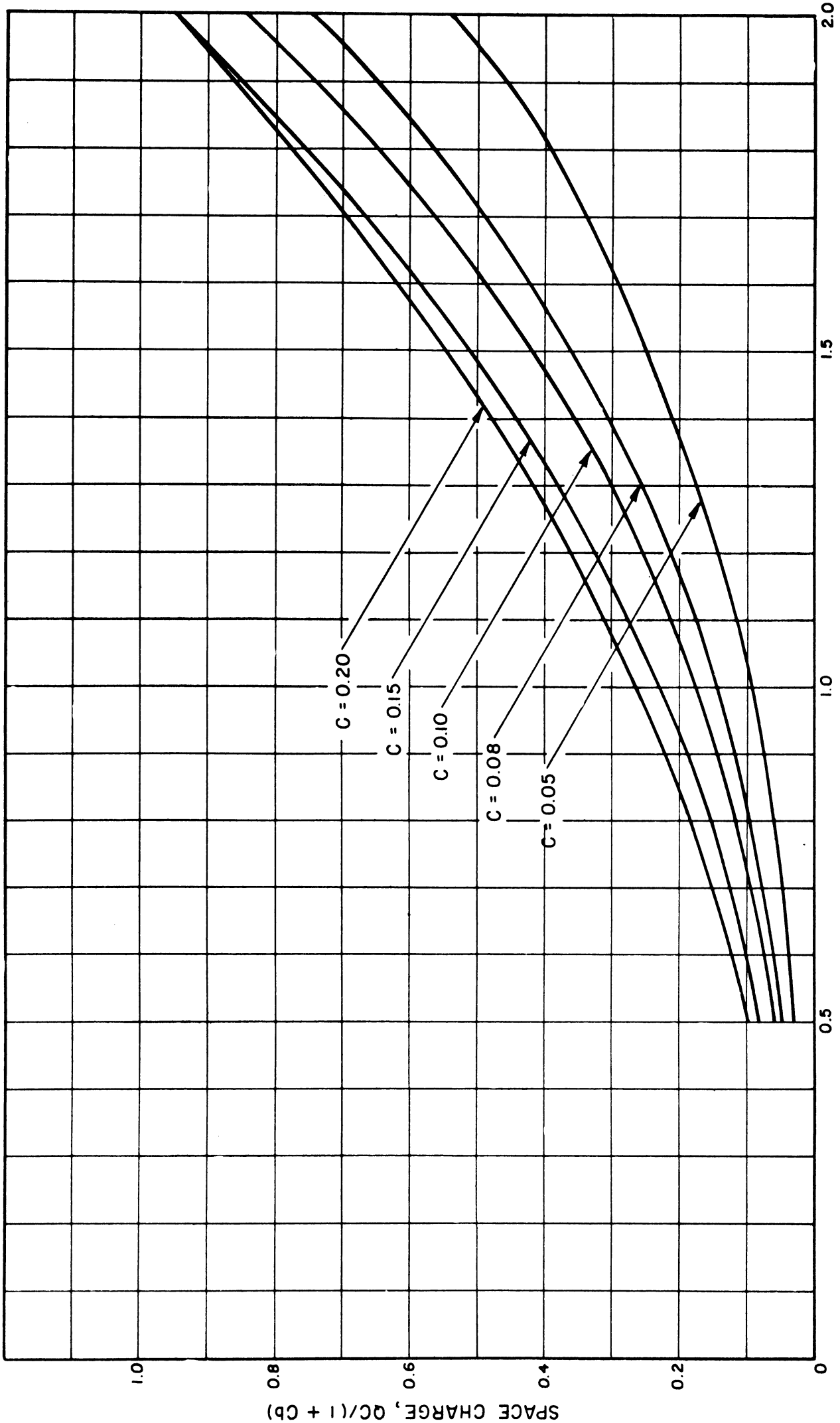

FIG. 5 SPACE CHARGE VS. BEAM DIAMETER FOR VARIOUS VALUES OF THE GAIN PARAMETER.
($a'/b' = 1.4$, $V_o = 2$ KV, DLF = 90 %)

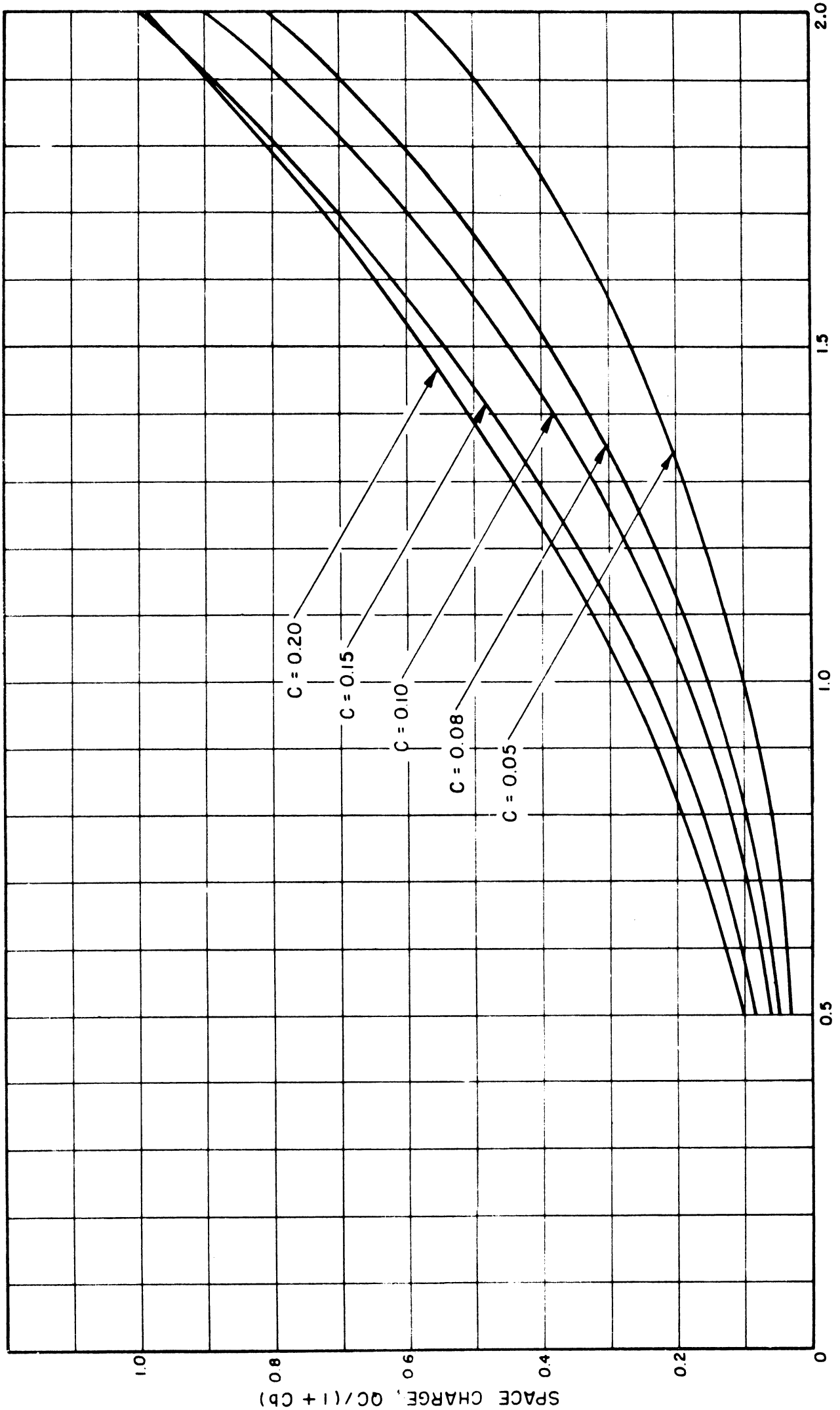

FIG. 6 SPACE CHARGE VS. BEAM DIAMETER FOR VARIOUS VALUES OF THE GAIN PARAMETER.
($a'/b' = 1.4$, $V_0 = 3$ KV, DLF = 90 %)

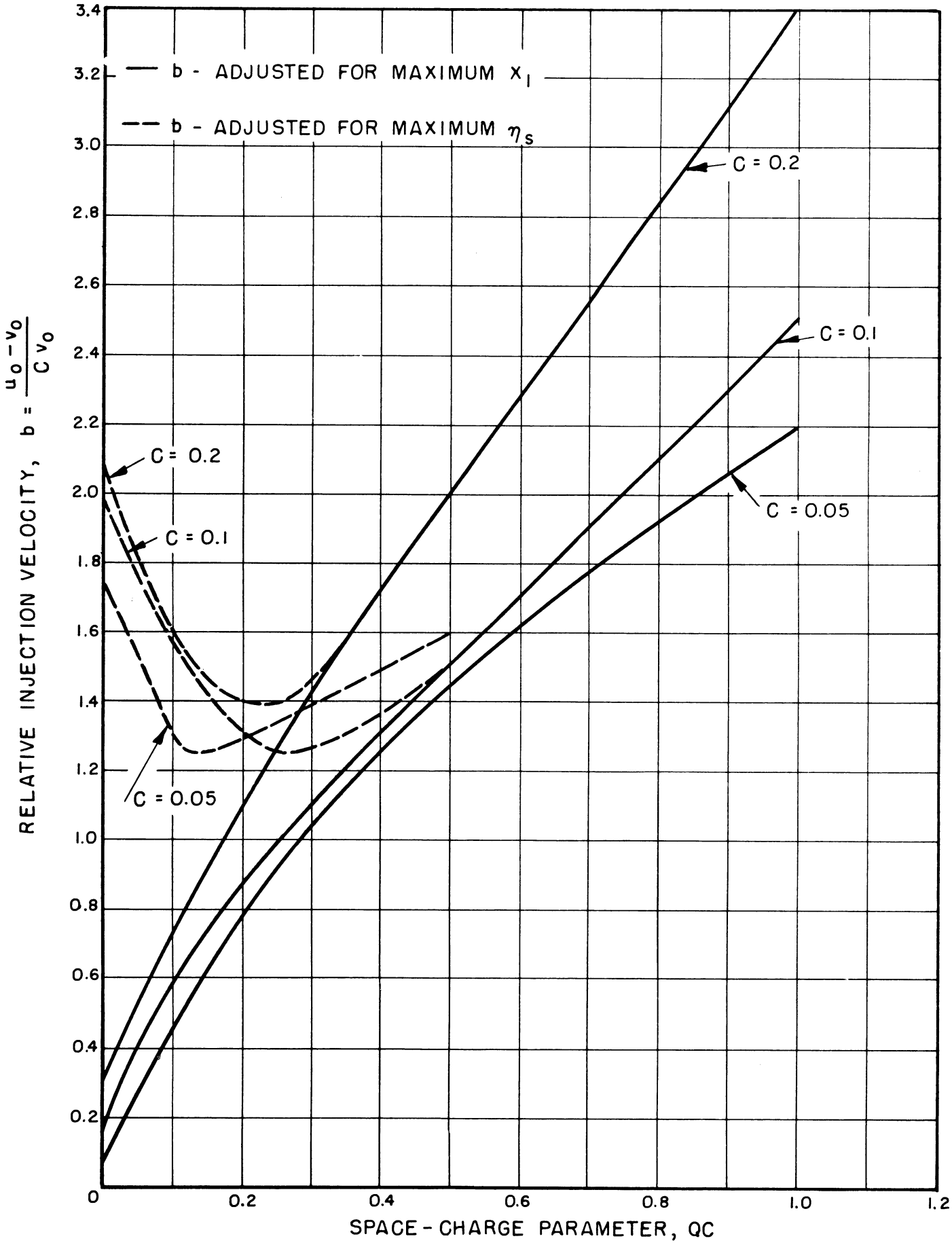

FIG. 7 RELATIVE INJECTION VELOCITY VS. SPACE-CHARGE PARAMETER. (B = 1, d = 0)

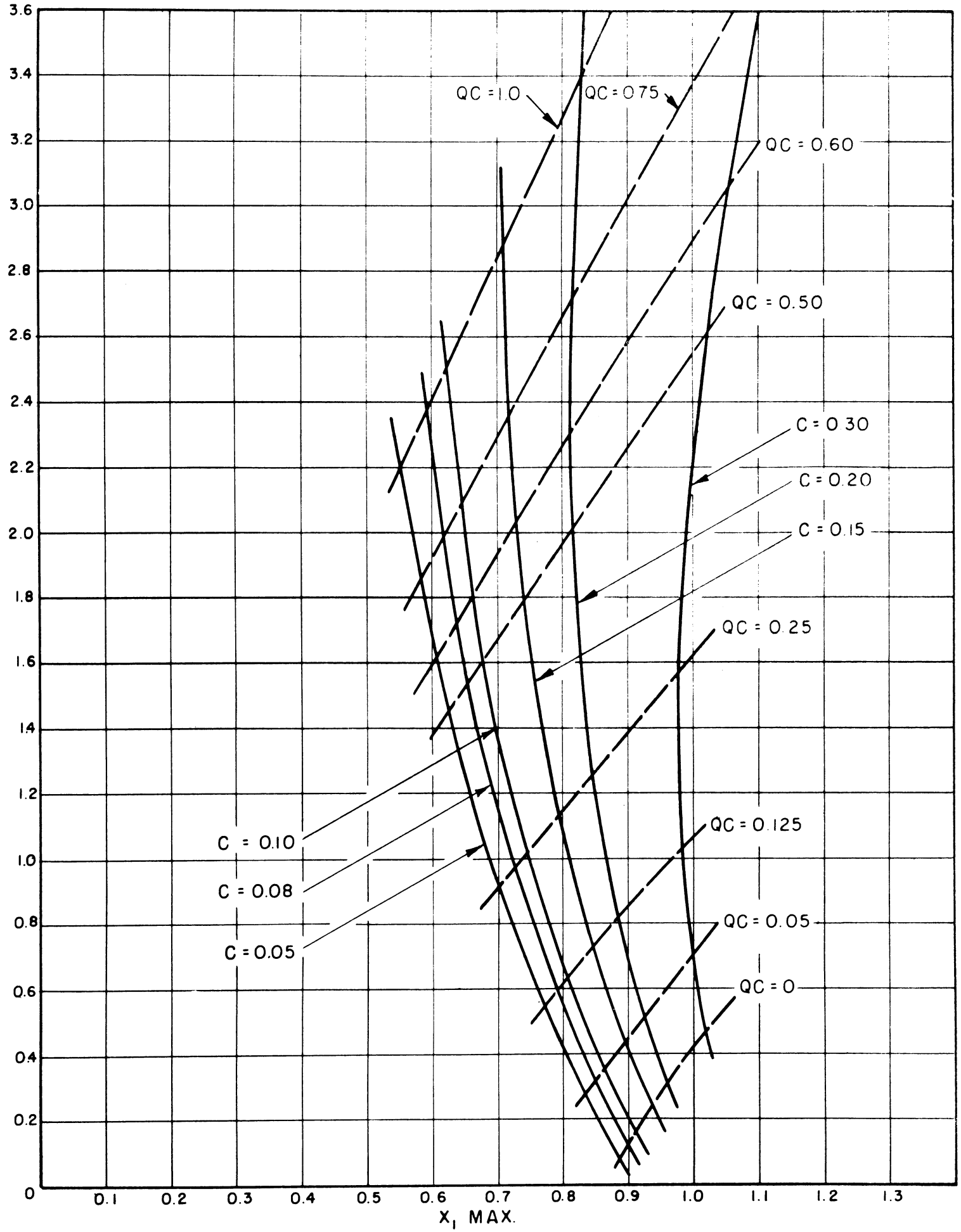

FIG. 8 b AT X_1 MAX. VS. X_1 MAX. WITH C AND QC AS PARAMETERS. (d = 0)

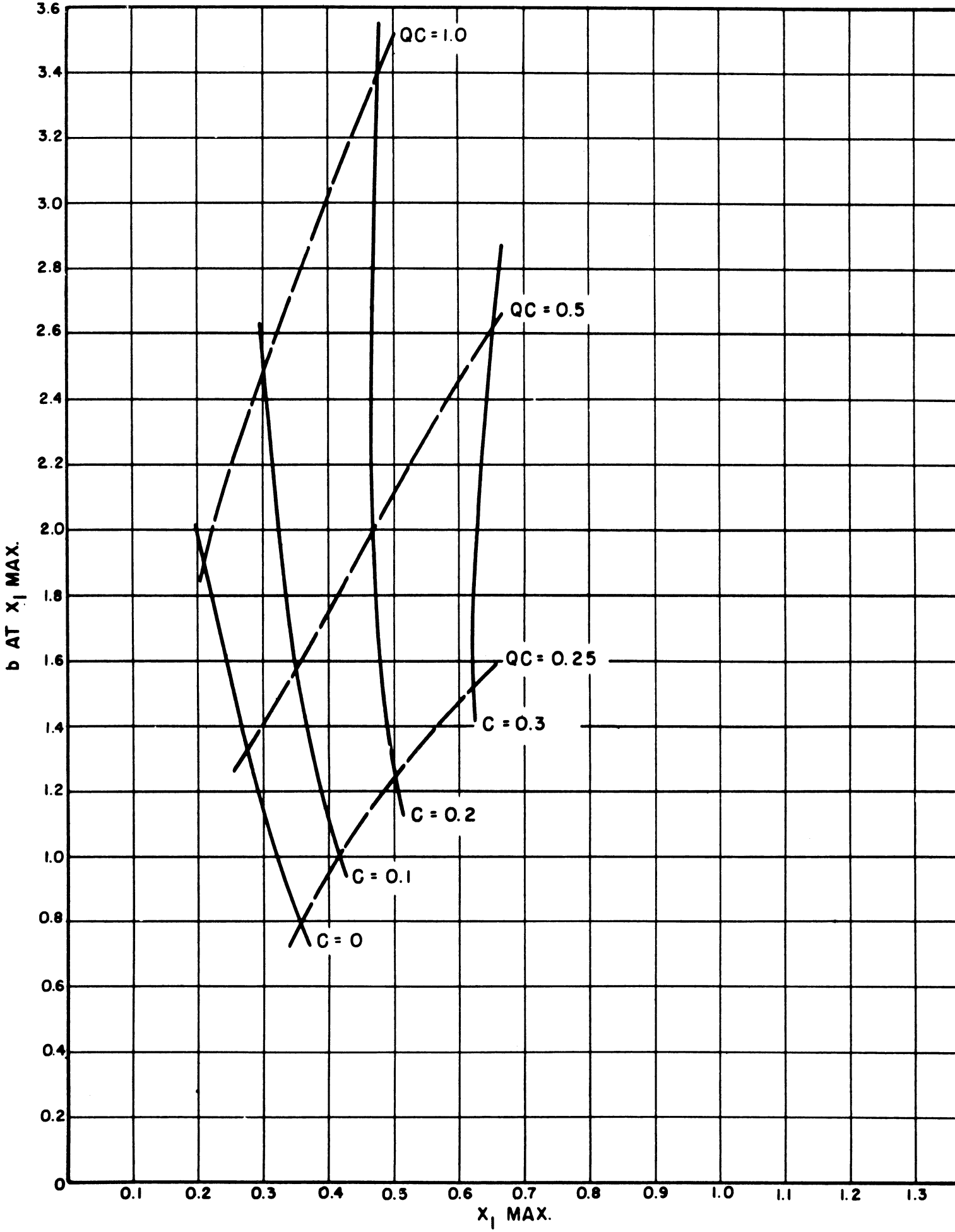

FIG. 9 b AT X_1 MAX. VS. X_1 MAX. WITH C AND QC AS THE PARAMETERS. (d = 1.0)

of b for maximum small-signal gain changes very little with increased loss but the value of $x_1$max. decreases nearly linearly with C at fixed QC. The data shown in Fig. 7 permit computation of the 1 + Cb correction factor and construction of a QC vs. QC/(1+Cb) curve (Fig. 10). It should be noticed that the correction factor is essentially independent of the velocity parameter b.

In Figs. 11 and 12, QC is plotted vs. B using the approximate form of Eq. 15 and also using the exact expression given in Eq. 14. Points have been calculated using this exact expression for QC for two different values of the velocity parameter b, (1) the value of b that gives maximum small-signal gain, and (2) the value of b that gives the maximum saturation efficiency. The 1 + Cb factor is important only for large values of B (beam diameter) and C (gain parameter) and may be omitted when $B < 1.0$ and $C < 0.1$. Comparison shows that the agreement between the exact and approximate expressions is essentially independent of a'/b' and V_o. It has also been found to be independent of the value of DLF. That the results are essentially independent of the value of b chosen is due to the fact that there is a factor 1 - Cy in the equation that nearly cancels out the influence of the 1 + Cb term. The y used is a negative number and varies as b does.

An alternative expression to Eq. 13 may be found by solving Eq. 10:

$$\omega_p/\omega = \frac{2C\,(QC)^{1/2}}{\left[1 - 2C\,(QC)^{1/2}\right] R_h} . \qquad (16)$$

Equating the expressions for ω_p/ω in Eqs. 13 and 16 and solving for P_μ gives

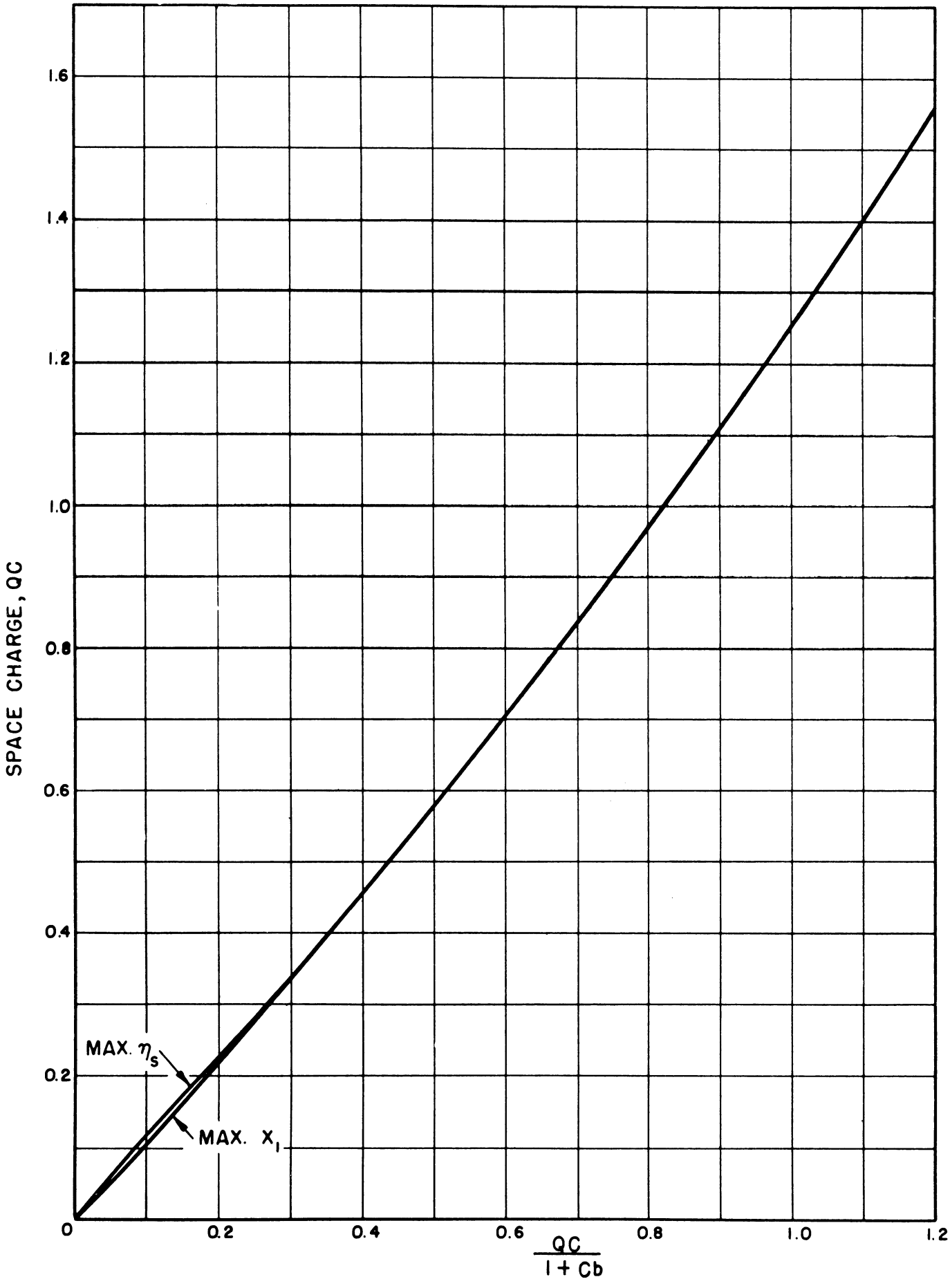

FIG. 10 SPACE-CHARGE CORRECTION. (C = 0.10, d = 0)

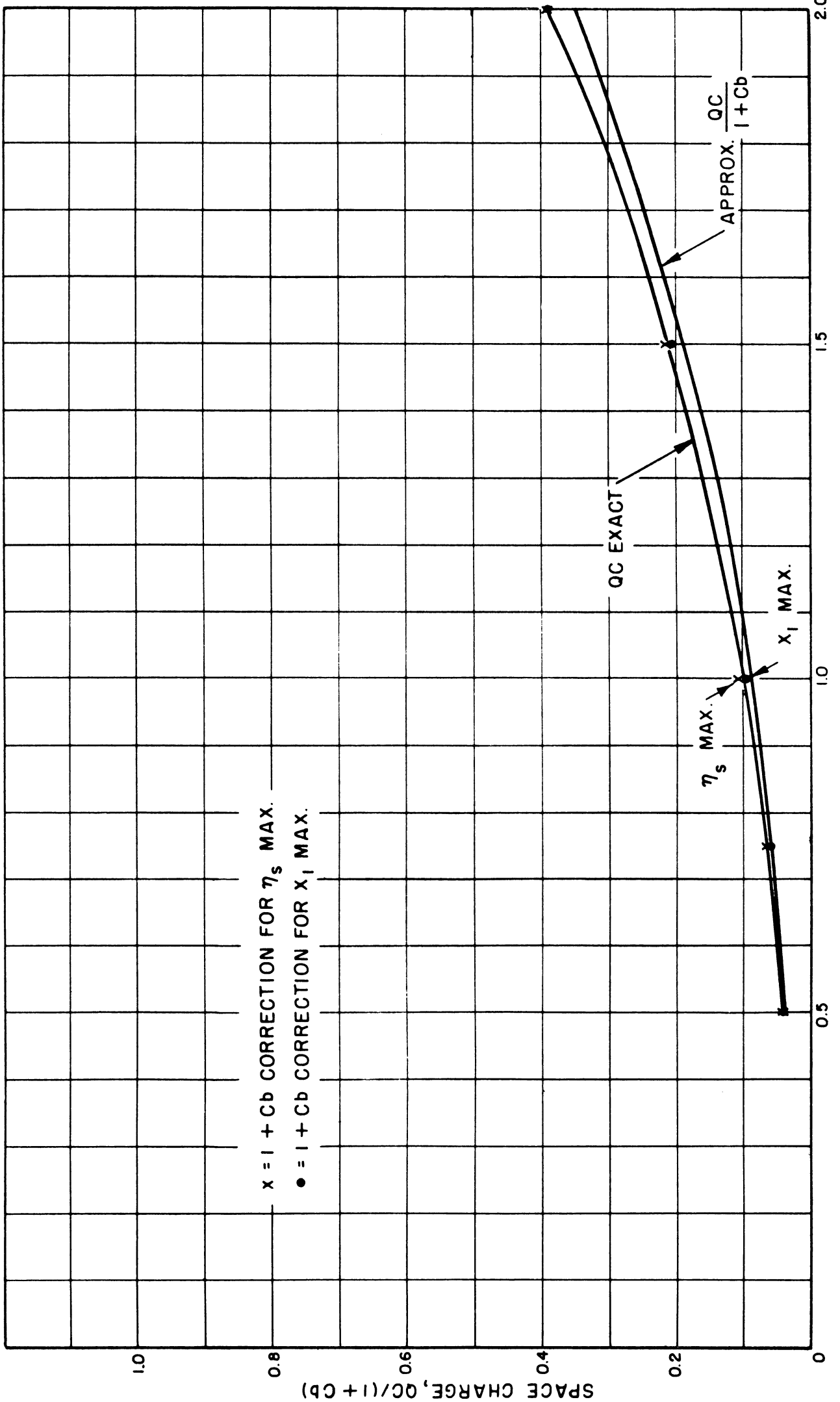

FIG. 11 SPACE CHARGE VS. BEAM DIAMETER FOR VARIOUS VALUES OF THE GAIN PARAMETER. (C = 0.10, a'/b' = 1.2, V_o = 1 KV, DLF = 90 %)

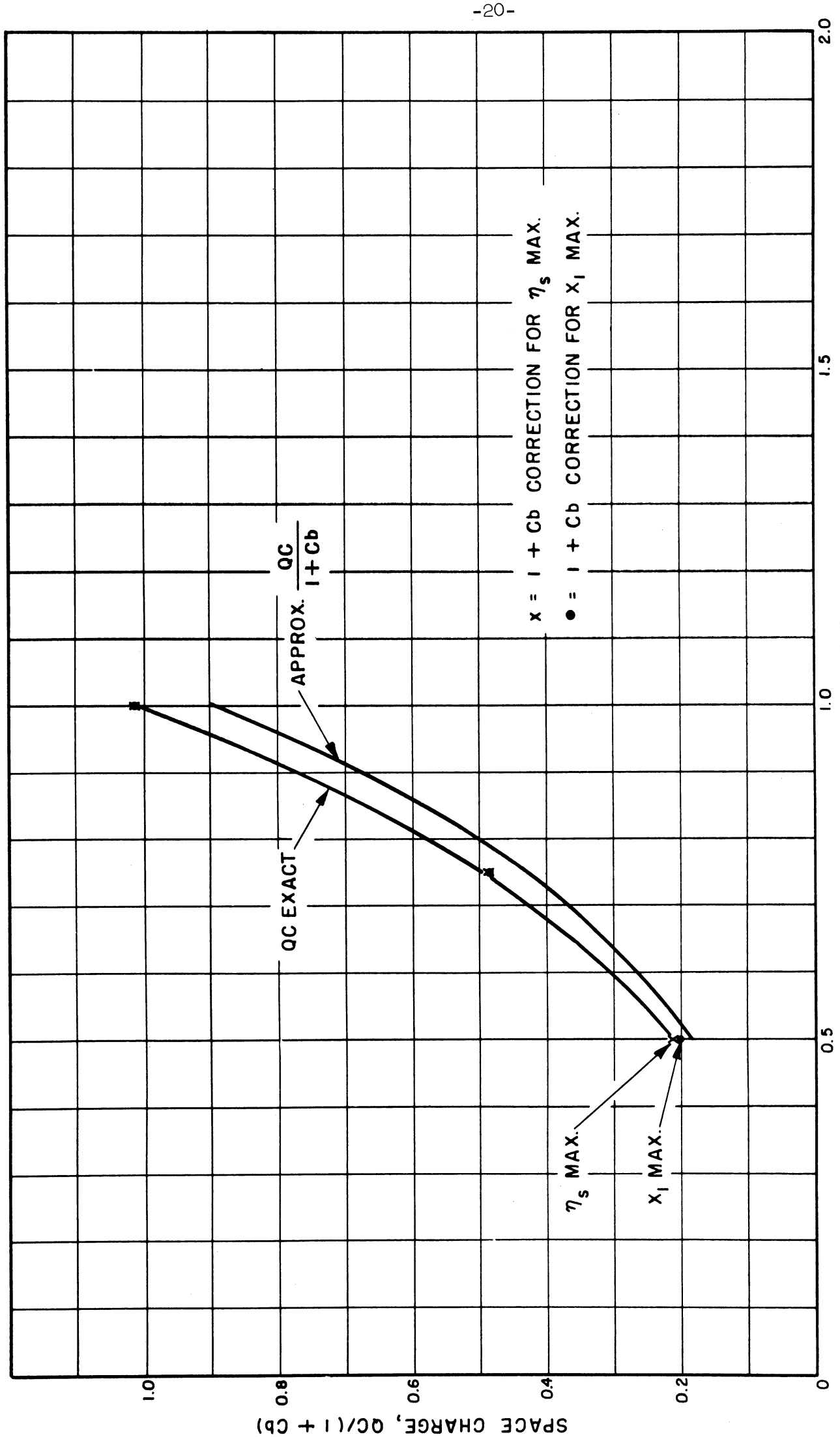

FIG. 12 SPACE CHARGE VS. BEAM DIAMETER FOR VARIOUS VALUES OF THE GAIN PARAMETER.
(C = 0.10, a'/b' = 2.0, V_0 = 10 KV, DLF = 90 %)

$$P_\mu = \frac{132.11\ (CB)^2\ (QC)}{\left[1 - 2C\ (QC)^{1/2}\right]^2 R_h^{\,2}\ (1 - Cy)^2} \cdot \qquad (17)$$

Equation 17 may be simplified by assuming that the quantity $(1-Cy)^2$ may be replaced by $(1+Cb)^2$:

$$(1 + Cb)^2\ P_\mu = \frac{132\ (CB)^2\ (QC)}{\left[1 - 2C\ (QC)^{1/2}\right]^2 R_h^{\,2}} \cdot \qquad (18)$$

From the above expression for P_μ, curves of the beam perveance vs. the beam diameter B are computed and shown in Figs. 13 and 14 for representative values of the parameters. It is seen from Eq. 17 that these curves are independent of V_o and dielectric loading. A correction factor for use in determining a more accurate value of the beam perveance when Cb is not small compared to unity has been calculated assuming that the quantity $(1-Cy)^2$ in Eq. 17 may be replaced by $(1+Cb)^2$. The perveance correction factor curve is shown in Fig. 15, where it is seen that for values of QC less than 0.5 the correction factor is critically dependent upon the value of b chosen.

DEPENDENCE ON HELIX VOLTAGE

The basic design curves of Figs. 5 and 6 show the variation of $QC/(1+Cb)$ with the beam diameter for particular values of the helix voltage V_o. No curves of this type were calculated for values of $QC > 1.0$, since the saturation efficiency decreases rapidly at large values of QC. In the curves shown it can be seen that for a given helix voltage V_o and a particular value of the beam diameter B the space-charge parameter increases

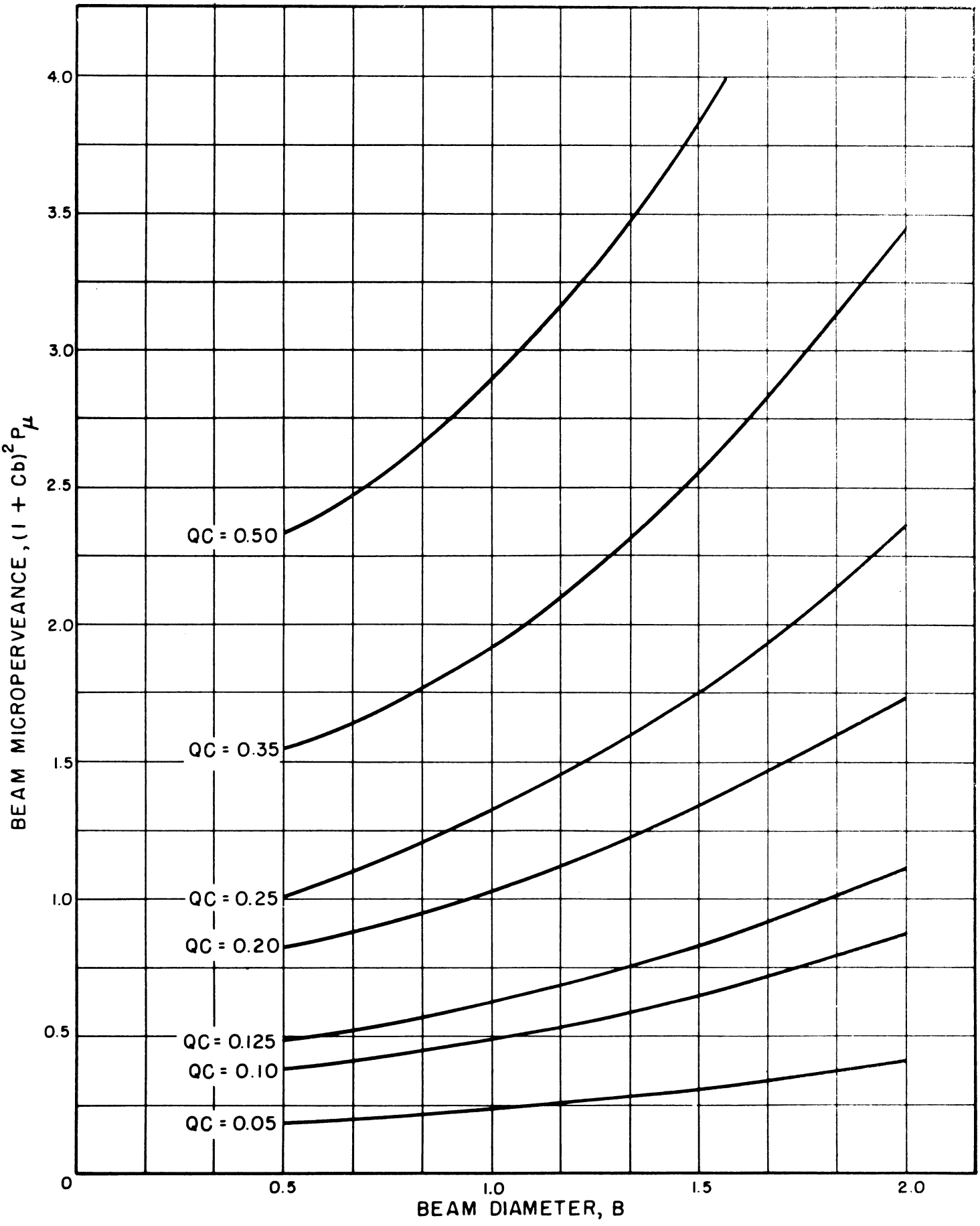

FIG. 13 MICROPERVEANCE VS. BEAM DIAMETER FOR VARIOUS VALUES OF THE SPACE-CHARGE PARAMETER. (C = 0.10, a'/b' = 1.4)

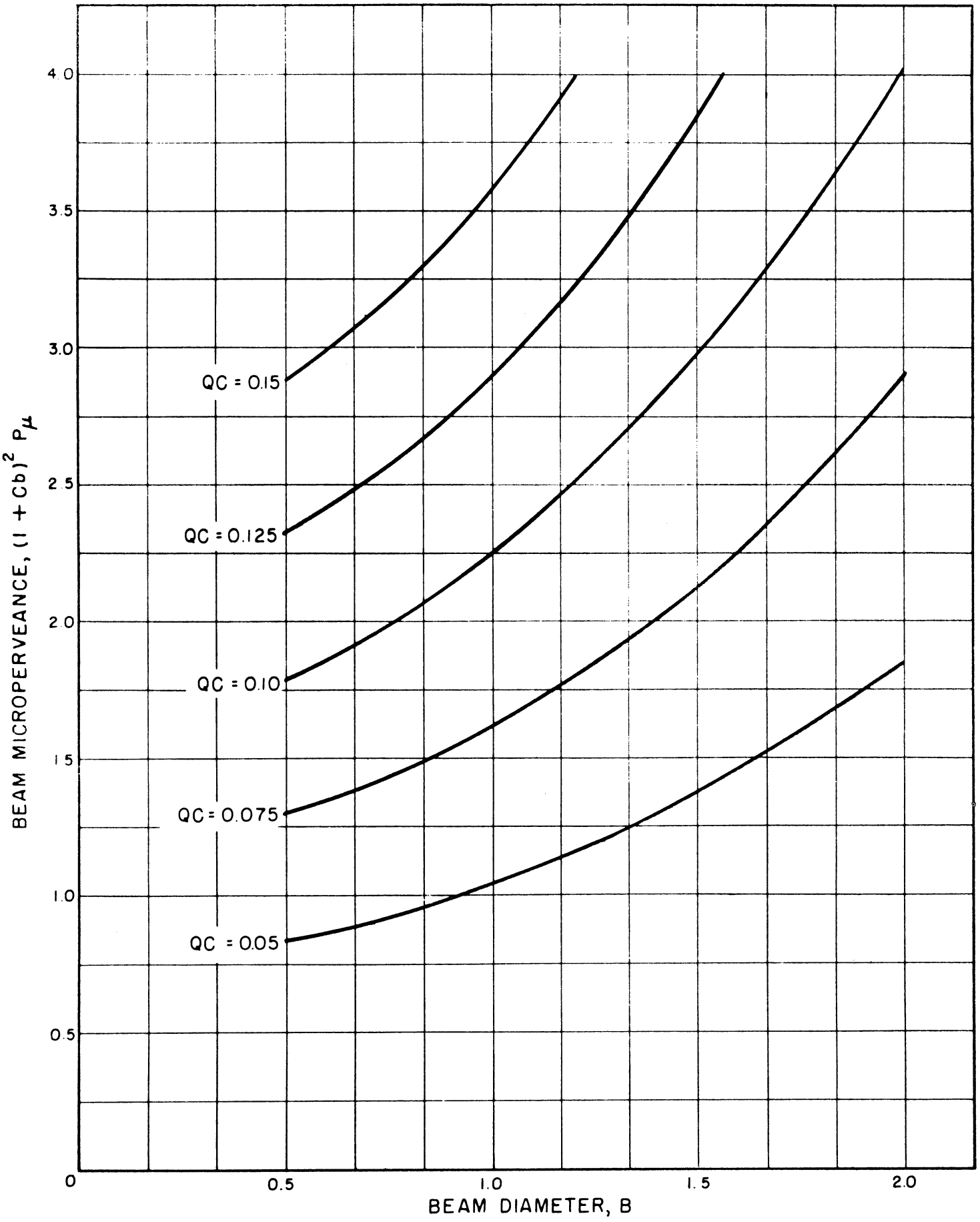

FIG. 14 MICROPERVEANCE VS. BEAM DIAMETER FOR VARIOUS VALUES OF THE SPACE-CHARGE PARAMETER. (C = 0.20, a'/b' = 1.4)

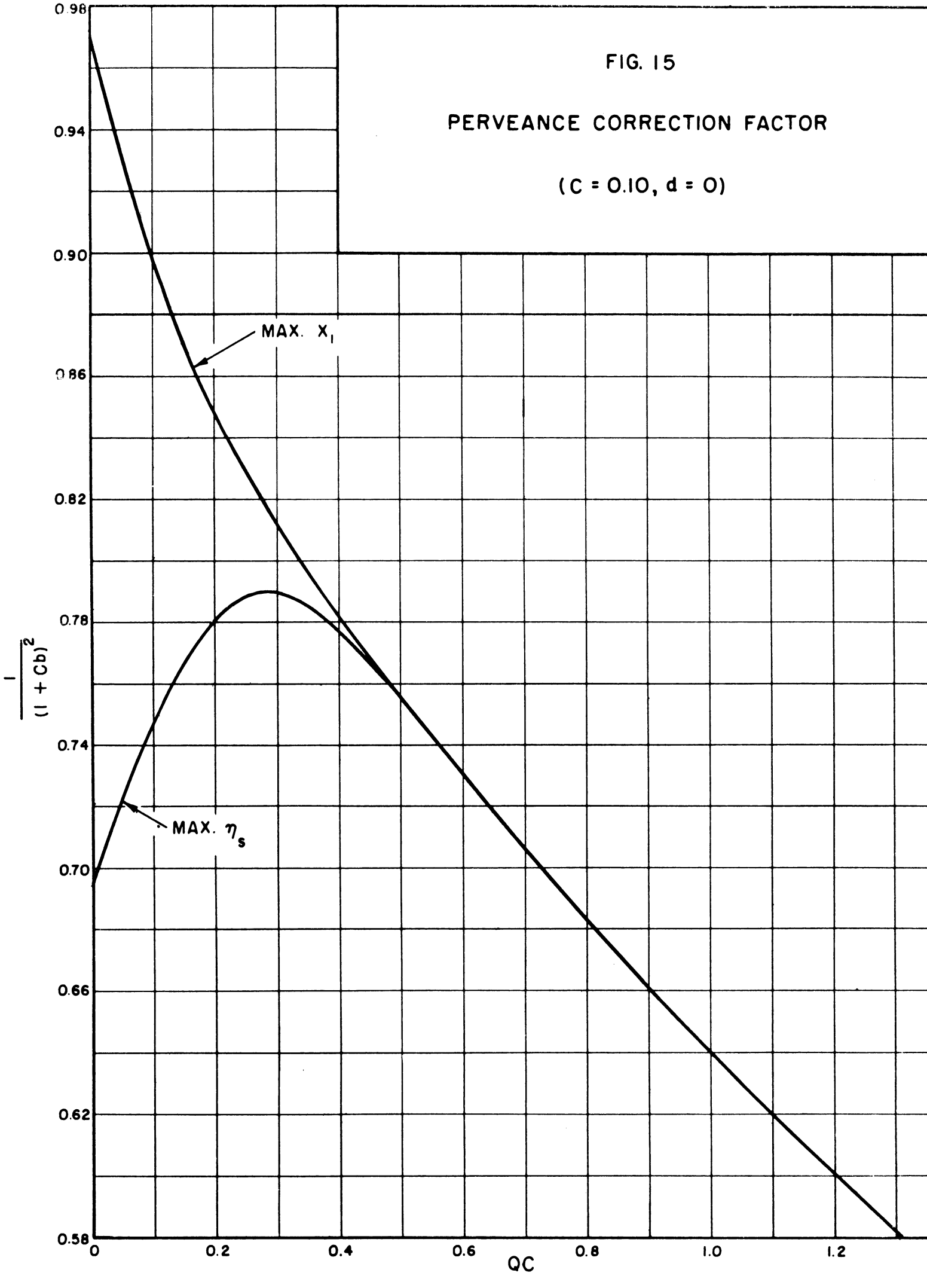
FIG. 15
PERVEANCE CORRECTION FACTOR
(C = 0.10, d = 0)
MAX. X_1
MAX. η_s
$\frac{1}{(1+Cb)^2}$
0.98
0.94
0.90
0.86
0.82
0.78
0.74
0.70
0.66
0.62
0.58
0
0.2
0.4
0.6
0.8
1.0
1.2
QC

rapidly as the ratio of helix-to-beam radii is increased. Since b' is fixed by B, this implies that QC increases as the helix radius is made larger. As long as the gain parameter is maintained constant the increase in QC must be due to an increase in the value of the plasma-frequency reduction factor, and hence an increase in the effective plasma frequency. In the limit, when the helix is removed to infinity, the reduction factor is unity and $\omega_q = \omega_p$.

Typical values of B for maximum theoretical efficiency in existing tubes are around 1.0, and it is not desirable to have $a'/b' > 1.4$ to 1.6 because of the resultant high values of QC and consequent lowering of efficiency. The lower limit on a'/b' is determined by the degree of beam interception and the tendency to backward-wave oscillate due to extremely tight coupling between the circuit and stream.

The dependence of the space-charge parameter on the helix voltage can be seen by plotting $QC/(1+Cb)$ vs. V_o for particular values of the beam diameter, as is done on an expanded scale in Figs. 16 and 17 for DLF = 90 percent. From these results it is apparent that the variation with voltage is most significant at large beam diameters. When B = 1.0 the space-charge parameter increases by approximately 40 percent for a 10-to-1 change in voltage. As the voltage is increased the term FI_o in Eq. 8 must increase at the same rate in order to keep C constant. Since B is fixed R_h remains constant. The impedance reduction factor F decreases as V_o is increased at fixed $\gamma a'$; hence I_o must increase at a greater rate than the voltage does to keep C constant. This increase in I_o results in an increasing QC with voltage. The variation of F with B is greatest at relatively high values of B.

The maximum helix voltage that may be used (which determines the retarded wavelength) is dependent upon several factors and therefore cannot

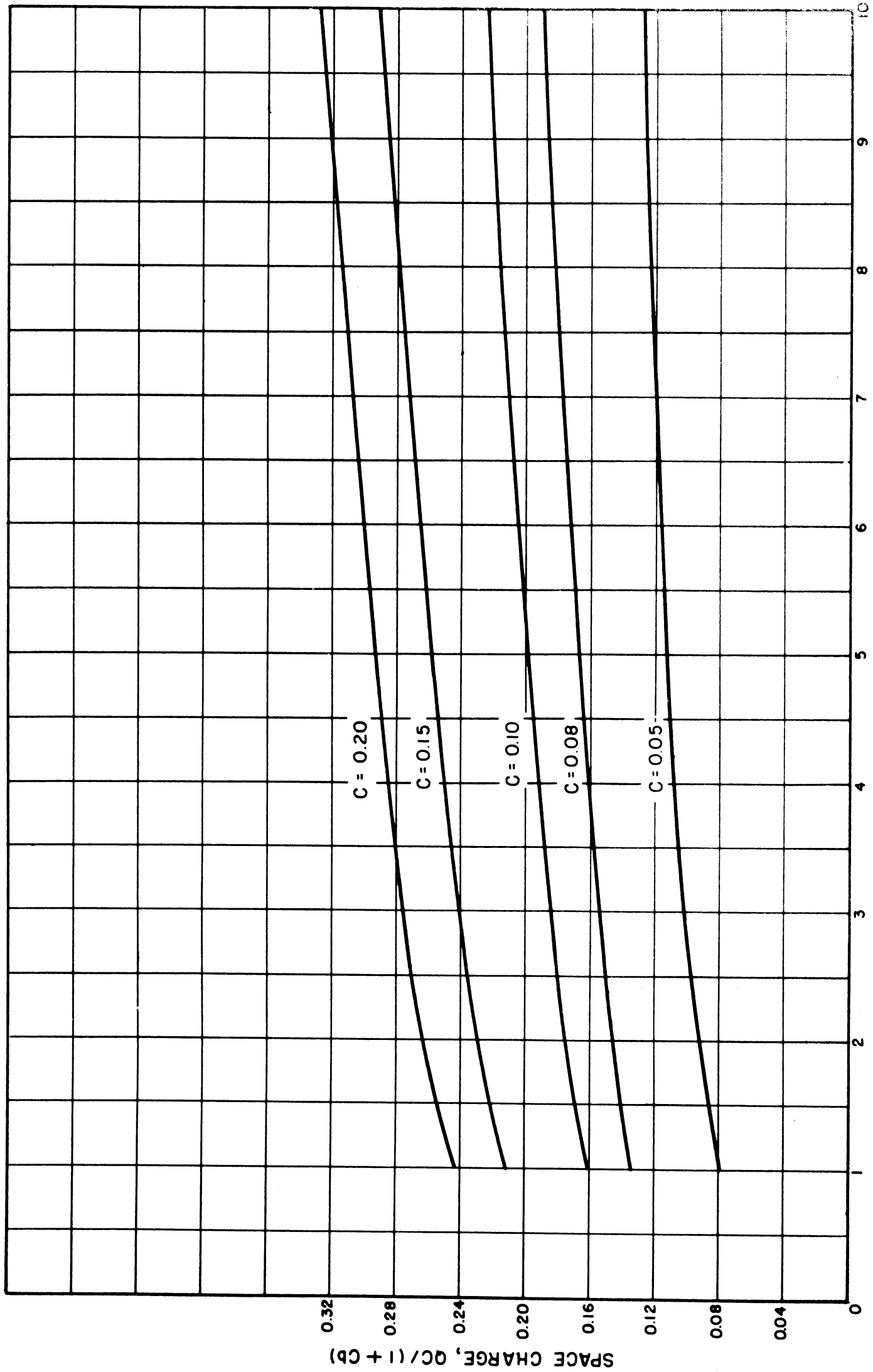

FIG. 16 SPACE CHARGE VS. HELIX VOLTAGE FOR VARIOUS VALUES OF THE GAIN PARAMETER.
(a'/b' = 1.4, R = 100, DLF = 90 %)

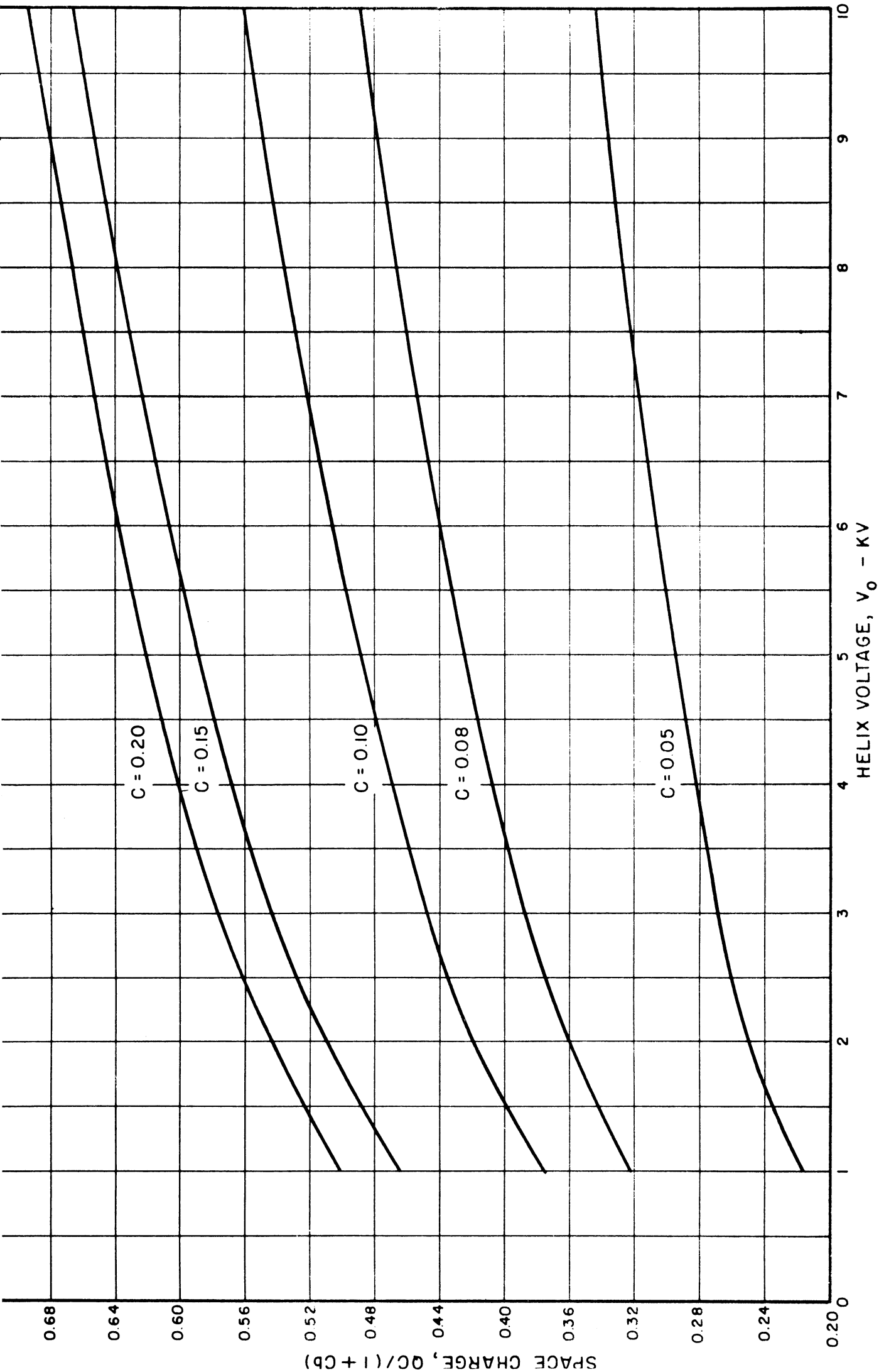

FIG. 17 SPACE CHARGE VS. HELIX VOLTAGE FOR VARIOUS VALUES OF THE GAIN PARAMETER.
(a'/b = 1.4, B = 1.50, DLF = 90 %)

be rigidly set. As the operating helix voltage and helix diameter are increased at any given frequency, the pitch of the helix increases, and it can be shown that the fundamental impedance is lowered and the effect of the harmonic fields is increased. The presence of a dielectric or metal shield surrounding the helix also influences the maximum usable helix voltage. Of course some of these difficulties can be overcome by using multi-filar or cross-wound helices.

Because of the above adverse effects, the maximum useful operating voltage for a unifilar helix is between 10 and 15 kv.

UNIVERSAL HELIX-DLF CURVE

One of the two reduction factors used in determining the actual helix impedance from the sheath-helix impedance depends upon the DLF. The DLF is defined mathematically by Tien[10] for helices of the same radii and $\gamma a'$ as

$$\text{DLF} \triangleq \frac{\cot \psi_{\text{ahwd}}}{\cot \psi_{\text{sh}}} , \tag{19}$$

where (ahwd) refers to the actual helix with dielectric and

(sh) refers to the sheath helix in free space.

Since the pitch distance for any helix is given by $2\pi a' v_o/c$, Eq. 19 may be written as

$$\text{DLF} = \frac{2\pi a'}{(\text{pitch}) \cot \psi_{\text{sh}}} . \tag{20}$$

The DLF for a particular helix may be calculated from Eq. 20 using the value of $\cot \psi_{\text{sh}}$ found from Fig. 18 for a particular $\gamma a'$. Both $\gamma a'$ and ka' may

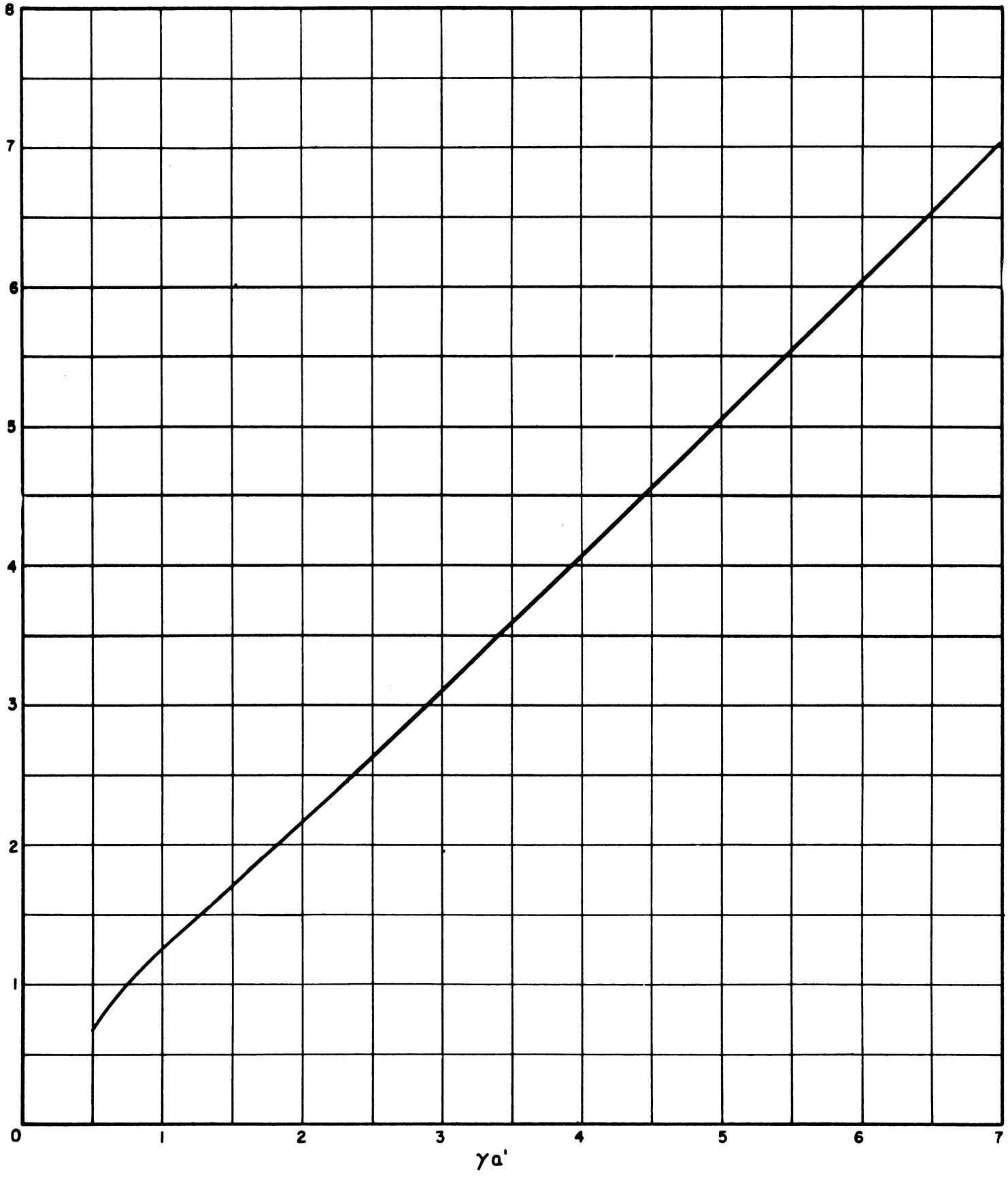

FIG. 18 $ka' \cot \psi_{sh}$ VS. $\gamma a'$ FOR A SHEATH HELIX.

be calculated on the basis of a measurement of the phase velocity along the actual helix in the presence of the dielectric at a given frequency. This measurement may be accomplished by any of the standard techniques.

In the design of traveling-wave tubes it is necessary to calculate the pitch or turns per unit length of the helix assuming a value for the DLF. Equation 20 can be written as

$$\frac{\text{DLF}}{ka'} = \frac{2\pi a'}{\text{pitch}\,(ka' \cot \psi_{sh})} \,. \tag{21}$$

With the aid of Fig. 18 and Eq. 21, a universal DLF curve is plotted. This universal curve, Fig. 19, permits calculation of the DLF from experimental data on the helix phase velocity and also calculation of the helix pitch for a given DLF and $(\gamma a')_{ah}$.

EXTENSION TO PERIODICALLY LOADED WAVEGUIDES AND MODIFIED HELIX STRUCTURES

In applications of traveling-wave tubes where the bandwidth needed is less than can be obtained with a nondispersive helical slow-wave structure but the peak or average power requirement is greater than a helix tube can yield due to thermal limitations of the helix, it is frequently desirable to employ some one of the varied forms of the periodically loaded waveguide or other dispersive structure. For many of these structures, such as the contra-wound helix[11] structure, the impedance vs. frequency relationship may be expressed as a constant times the sheath-helix impedance. The procedure developed here will be to relate the structure impedance to the sheath-helix impedance by an impedance gain factor, G, which in general is a function of frequency. This is similar to the determination of the actual helix impedance from the sheath-helix impedance using the impedance reduction factor.

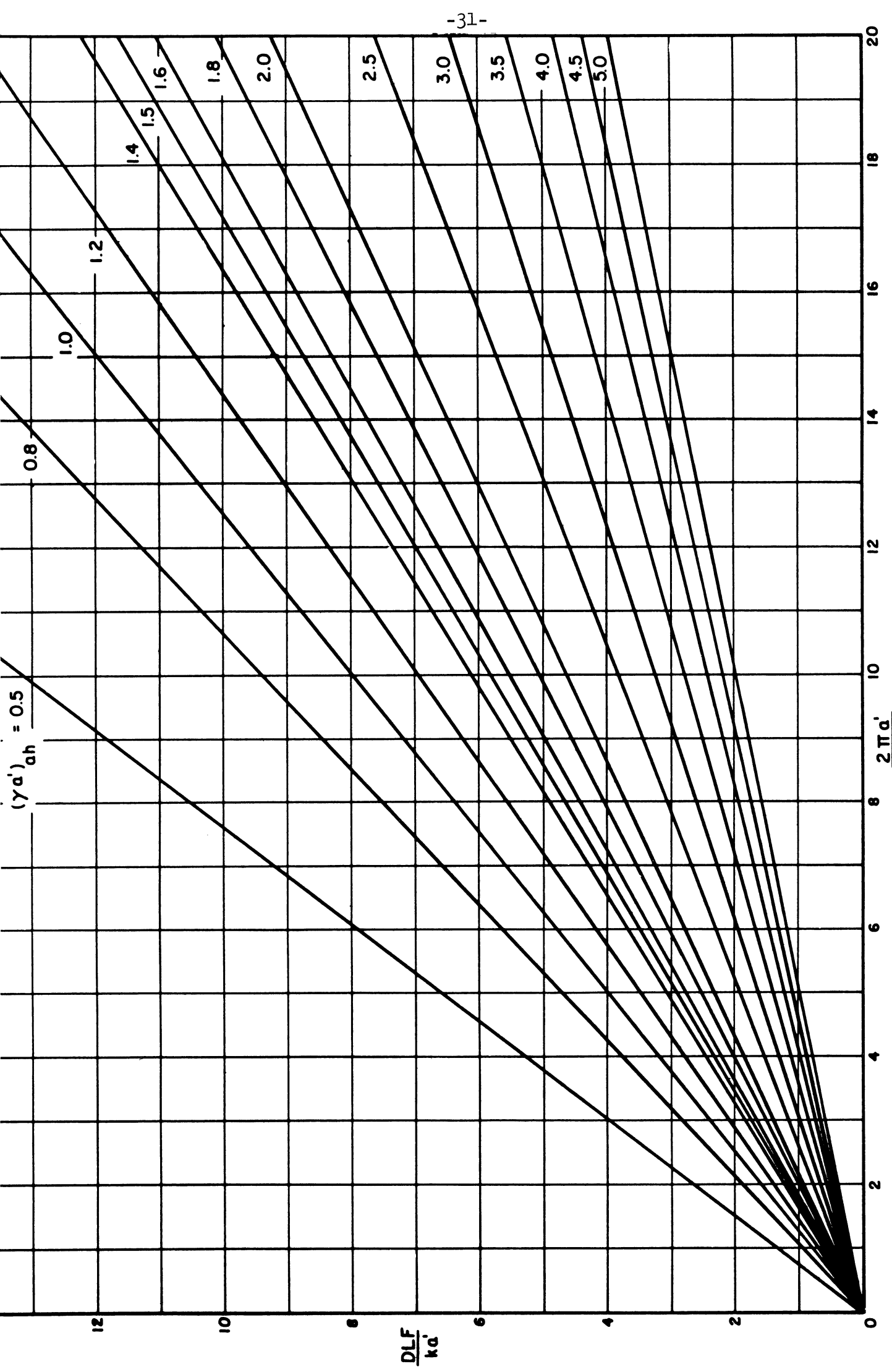

FIG. 19 HELIX DLF VS. PITCH AS A FUNCTION OF FREQUENCY

It is important to point out once again that the large-signal results apply to traveling-wave tubes independent of the r-f propagating structure as long as these structures can be represented by an equivalent circuit that is an LC transmission line even though L and C may both be functions of frequency. This is true because the circuit serves only to present a longitudinal electric field at the beam position and retard an electromagnetic wave. In the longitudinal theory the helix has been assumed nondispersive. In the event that the resonant or dispersive structure being used has an impedance curve that is not approximately parallel to that of the sheath helix, then G will be a function of $\gamma a'$ and hence of B.

The impedance gain factor will be defined in such a way that it takes into account the effect of the mounting method on the impedance.

The structure impedance is written as

$$K_d = G\, K_s \ , \tag{22}$$

where G = the impedance gain factor expressing the ratio of the structure impedance mounted in the vacuum envelope to the sheath-helix impedance.

Proceeding through the derivation using the above impedance relation and assuming the same values of C and B for the dispersive structure as for the helix yields, in place of Eqs. 14 and 15,

$$(QC)_d = \frac{60}{\left[\frac{B}{R_d}\left(\frac{G\, K_s'}{C}\right)^{1/2} \frac{(1 + Cb)^{1/2}}{1 - Cy} + 15.5\, C\right]^2} \ , \tag{23}$$

and

$$(QC)_d = \frac{60\,(1 + Cb)}{\left[\frac{B}{R_d}\left(\frac{G\,K_s'}{C}\right)^{1/2} + 15.5\,C\right]^2} \,. \tag{24}$$

For periodically loaded waveguide structures the dielectric loading factor is unity and the geometric reduction factor on the radian plasma frequency is different from that for the helix tube. The plasma-frequency reduction factor will generally be larger for loaded-waveguide structures than for the helix, since the effective circuit radius will be somewhat greater than the radius of the center hole in the structure for the beam. The ratio of $(QC)_d$ to $(QC)_h$ can be written as

$$\frac{\left[\frac{QC}{1 + Cb}\right]_d^{1/2}}{\left[\frac{QC}{1 + Cb}\right]_h^{1/2}} = \xi^{1/2}\,\frac{\left[1 + \frac{15.5\,C\,R_h}{\nu\,F^{1/2}}\right]}{\left[1 + \frac{15.5\,C\,R_d}{\nu\,G^{1/2}}\right]} \,, \tag{25a}$$

where

$$\xi \triangleq \left(\frac{R_d}{R_h}\right)^2 \frac{F}{G} \,, \tag{25b}$$

$$\nu \triangleq \left(\frac{B\,K_s'}{C}\right)^{1/2} \,, \tag{25c}$$

R_h = the radian plasma-frequency reduction factor for a helix of equivalent B and a'/b', and

R_d = the radian plasma-frequency reduction factor for the resonant or dispersive structure.

Since the second term in the denominator is small compared to unity, Eq. 25a is expanded in a power series, neglecting higher-order terms. The binomial series is used then to give the following expression:

$$\frac{\left[\frac{QC}{1 + Cb}\right]_d}{\left[\frac{QC}{1 + Cb}\right]_h} = \xi \left[1 + \frac{30.96\ C}{\nu}\left(\frac{R_d}{G^{1/2}}\right)\left(\frac{1}{\xi^{1/2}} - 1\right)\right] . \qquad (26)$$

The space-charge reduction factor for dispersive structures, ξ, defined in Eq. 25b, is shown in Fig. 20 for particular values of G and R_d/R_h. It is evident that the first-order correction term in Eq. 26 is negligible in most instances. If the radian plasma-frequency reduction factor is the same for the dispersive structure as for the helix, Eq. 26 may be written as

$$\frac{\left[\frac{QC}{1 + Cb}\right]_d}{\left[\frac{QC}{1 + Cb}\right]_h} \approx \frac{F}{G} = \xi \cdot (R_d = R_h). \qquad (27)$$

The value of G above includes the effect of dielectric loading when structures such as the contra-wound helix are used. Thus G is analogous to F G*, where in the presence of a dielectric F is the same as for a helix and G* is the impedance gain factor. In Fig. 21 is shown a graph of Eq. 25a for representative values of G and $R_d = R_h$. It is apparent that the F/G approximation is very good except for large values of B. The correction factor is somewhat dependent upon a'/b' but not on the voltage or DLF. The effect is also shown for large C.

Since the stream perveance, as expressed in terms of the design parameters in Eq. 21, is a function of the reduction factor R, there will also be a perveance correction factor for the structures where $R_d \neq R_h$.

The perveance expression for dispersive structures is, from Eq. 17,

$$P_\mu = \frac{132\ (CB)^2\ (QC)_d}{\left[1 - 2C\ (QC)_d^{1/2}\right] R_d^2\ (1 - Cy)^2} , \qquad (28)$$

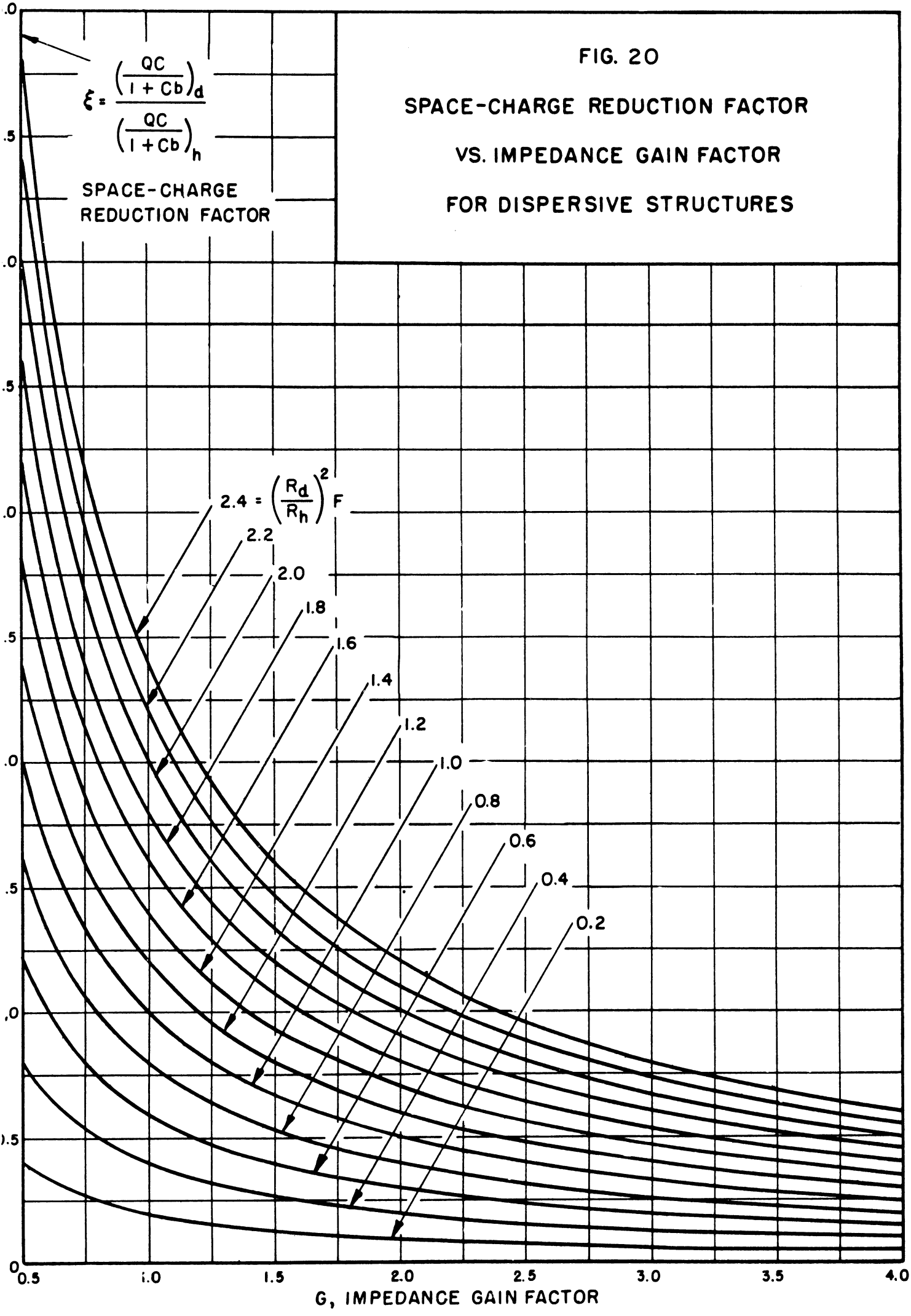
FIG. 20
SPACE-CHARGE REDUCTION FACTOR
VS. IMPEDANCE GAIN FACTOR
FOR DISPERSIVE STRUCTURES
$\xi = \frac{\left(\frac{QC}{1+Cb}\right)_d}{\left(\frac{QC}{1+Cb}\right)_h}$
SPACE-CHARGE REDUCTION FACTOR
$2.4 = \left(\frac{R_d}{R_h}\right)^2 F$
2.2
2.0
1.8
1.6
1.4
1.2
1.0
0.8
0.6
0.4
0.2
0.5
1.0
1.5
2.0
2.5
3.0
3.5
4.0
G, IMPEDANCE GAIN FACTOR

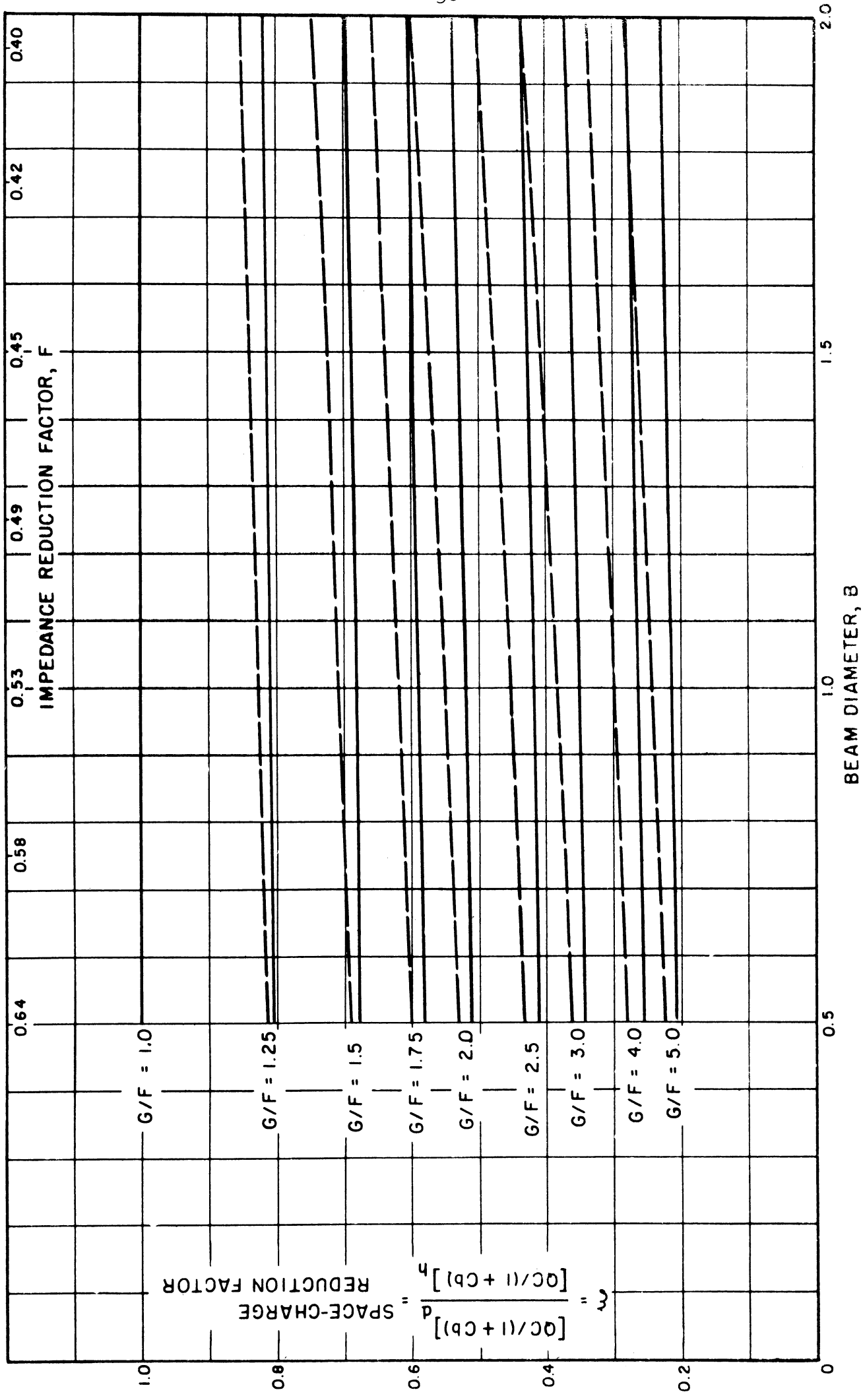

FIG. 21 SPACE-CHARGE REDUCTION FACTOR VS. BEAM DIAMETER. ($R_d = R_h$).
(C = 0.1 ——, C = 0.2 — — —, a'/b' = 1.2, V_o = 5 KV, DLF = 90 %)

where $(QC)_d = \xi\ (QC)_h$, the space-charge parameter for the dispersive structure, and

R_d = the plasma-frequency reduction factor for a dispersive structure.

Since the QC/(1+Cb) curves and the perveance curves have already been constructed for a helix structure, the design procedure will be to select the desired values of C, QC and B from the large-signal efficiency curves and then determine the equivalent space-charge parameter for the helix in order to use the existing curves. Thus the perveance curves are entered using $(QC)_h$ and the perveance correction factor is given by

$$\kappa = \frac{P_{\mu d}\ (1 + Cb)^2}{P_{\mu h}\ (1 + Cb)^2} = \left(\frac{R_h}{R_d}\right)^2 . \qquad (29)$$

PROCEDURE FOR USE OF DESIGN CURVES

General

Usually the desired power output (pulsed or cw) and operating frequency range are determined by the proposed use of the tube. The large-signal analysis as previously discussed is independent of the operating frequency and the operating structure and hence has a wide range of application. The choice of a particular structure is usually made on the basis of the power level expected and the desired bandwidth.

The design procedure is here outlined for a helix-type tube, but can be adapted for the design of other traveling-wave tube structures using the space-charge and perveance correction factors developed in the previous section. A flow diagram illustrating the design procedure using the three classes of curves, namely the efficiency, space-charge and perveance curves, is shown in Fig. 22. The procedure involves an iteration technique around

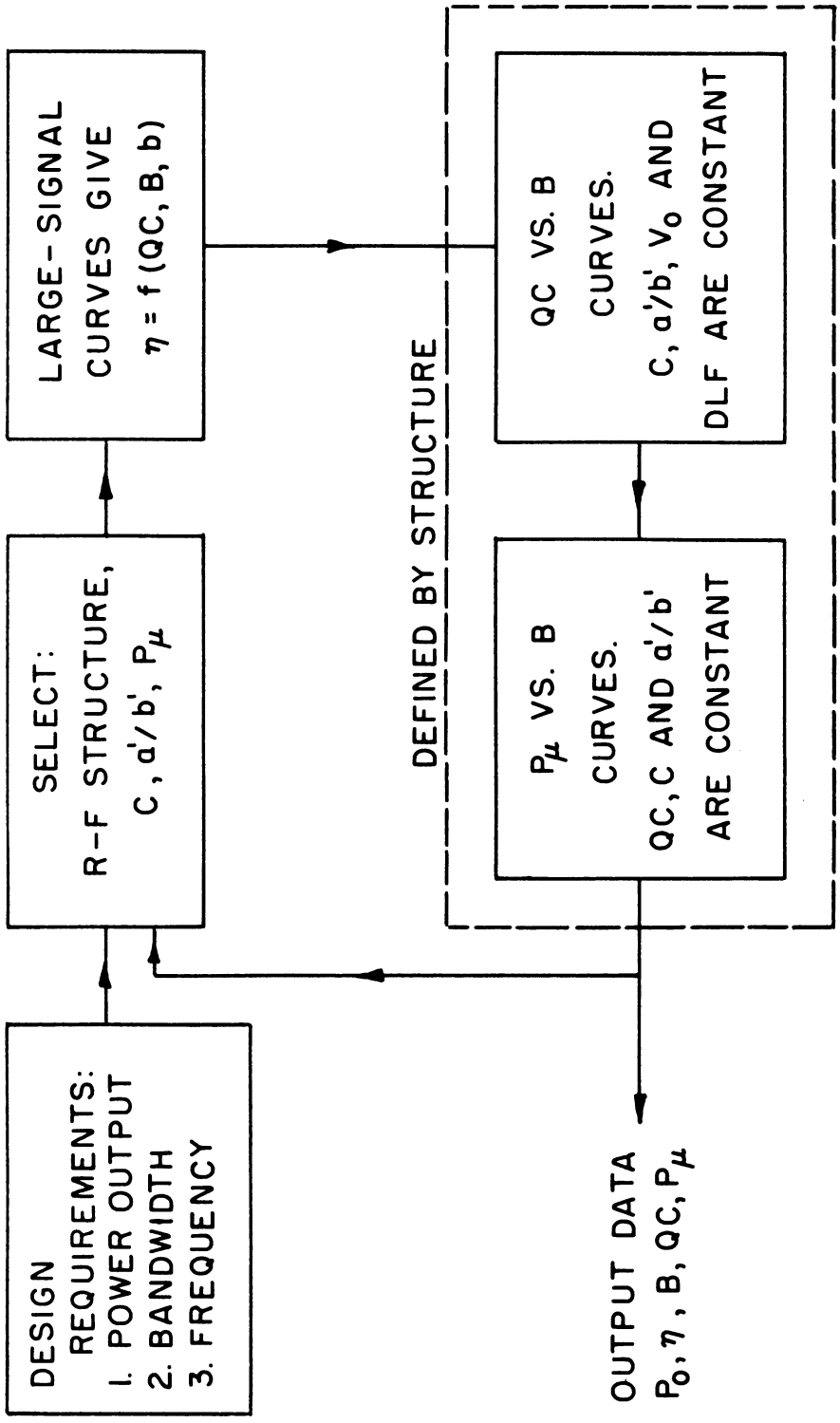

FIG. 22 FLOW DIAGRAM FOR TRAVELING-WAVE AMPLIFIER DESIGN PROCEDURE.

the loop indicated in the above figure. From the design requirements a structure and means of mounting is selected which in the case of the helix then determines the values of a'/b' and DLF. Also a realizable value of the gain parameter C is chosen consistent with operating frequency and efficiency requirements. This value of C is then used in conjunction with the efficiency curves to tentatively decide upon values for QC and B. The space-charge and perveance curves are then used to determine if the chosen parameters can be realized. If the combination of parameters selected is not realizable for the chosen r-f structure, a new value of QC associated with the perveance is taken and the iterative loop is traversed again. This process converges rapidly to a design consistent with physical limitations and design requirements.

Outline of Iterative Procedure

Once the power output, frequency range and type of structure have been selected, the procedure is according to the following steps.

1. The design is based on the given power output (P_o).
2. The large-signal efficiency curves, where efficiency is presented as a function of QC, B, d and b for various values of C, are used to select the operating parameters desired and to find an efficiency. Usually the d = 0 curves are used and then values of C, QC, B and b are found. The correction for loss is included at a later point. An idea of the ideal operating point is obtained from these curves; it now remains to see if these ideal parameters can be achieved simultaneously using a particular type of r-f structure.

   Values of B and QC are selected from the large-signal curves to give maximum saturation efficiency. There is a fairly broad plateau

in the efficiency curves around the maxima so that there is some freedom of choice. High gain per unit length and high efficiency require as large a value of C as can be realized. The selection of $B = \gamma b' = \gamma a' (b'/a')$ is also dependent upon the operating bandwidth desired, since the bandwidth for constant gain is dependent upon $\gamma a'$. For broad-band tubes the optimum $\gamma a'$ is around 1.8 and for highest saturation efficiency $B \approx 1.0$. Using these values of B and $\gamma a'$ would dictate a b'/a' of 0.56, which would result in a weak interaction between the circuit and stream, thus lowering the impedance C and the gain. A B = 1 and $b'/a' = 0.7$ would give considerably stronger interaction and result in $\gamma a' = 1.43$. It has been found in this laboratory, experimentally, that operation over a 1.5 to 1 frequency range can be obtained at s-band with this value of $\gamma a'$. The tendency for a particular tube to backward-wave oscillate and the feasibility of using mode suppression techniques will determine the maximum usable b'/a' ratio.

Values of C, QC, B, b, a'/b' and DLF are tentatively selected. Then from the large-signal curves a theoretical saturation efficiency is found. Thus the beam power may be calculated on the basis of the theoretical efficiency and the power output P_o.

Practical values of a'/b' lie somewhere between 4/3 and 2. It was pointed out earlier that the large-signal results are relatively independent of a'/b'.

3. The next step in the design procedure is to consult a curve or nomograph of V_o vs. I_o with beam perveance and beam power as the parameters. From this curve the other beam quantities can be determined

using the beam power as calculated in (2) above and assuming a value of beam perveance or beam potential, since the beam power and an assumed value of perveance will automatically determine V_o and I_o. On the other hand, the beam perveance and beam current are also explicitly determined by the beam power and a chosen value of V_o. Whether beam voltage or beam perveance is selected as the independent variable depends upon the limitations encountered in the electron gun design. The perveance is in general limited by the type of electron gun used and the limitation on emission density imposed by the duty cycle. The beam voltage, V_o, is usually limited by power supply requirements and voltage breakdown between electron gun electrodes.

In applications of traveling-wave tubes where minimum weight of the tube and its solenoid are of primary importance, the type of focusing to be employed will be influential in the choice of electron gun perveance and voltage. The minimum magnetic field required for focusing (Brillouin flow)[12] is shown in Fig. 23 as a function of the voltage and perveance. For magnetic field strengths greater than that required for Brillouin flow the space-charge wave propagation could be affected and QC increased through an increase in the magnitude of the plasma-frequency reduction factor[13].

4. The next step is to check the assumption on QC, B and C. Several steps are required. First decide whether the design is to be based on b for maximum small-signal gain or on b for maximum saturation efficiency. This determines the (1+Cb) correction factor. It should be recalled that $\gamma a'$ is equal to a'/b' times B. It is well known that $\gamma a'$ is selected on a compromise basis since both wideband operation and high circuit impedance are desired simultaneously.

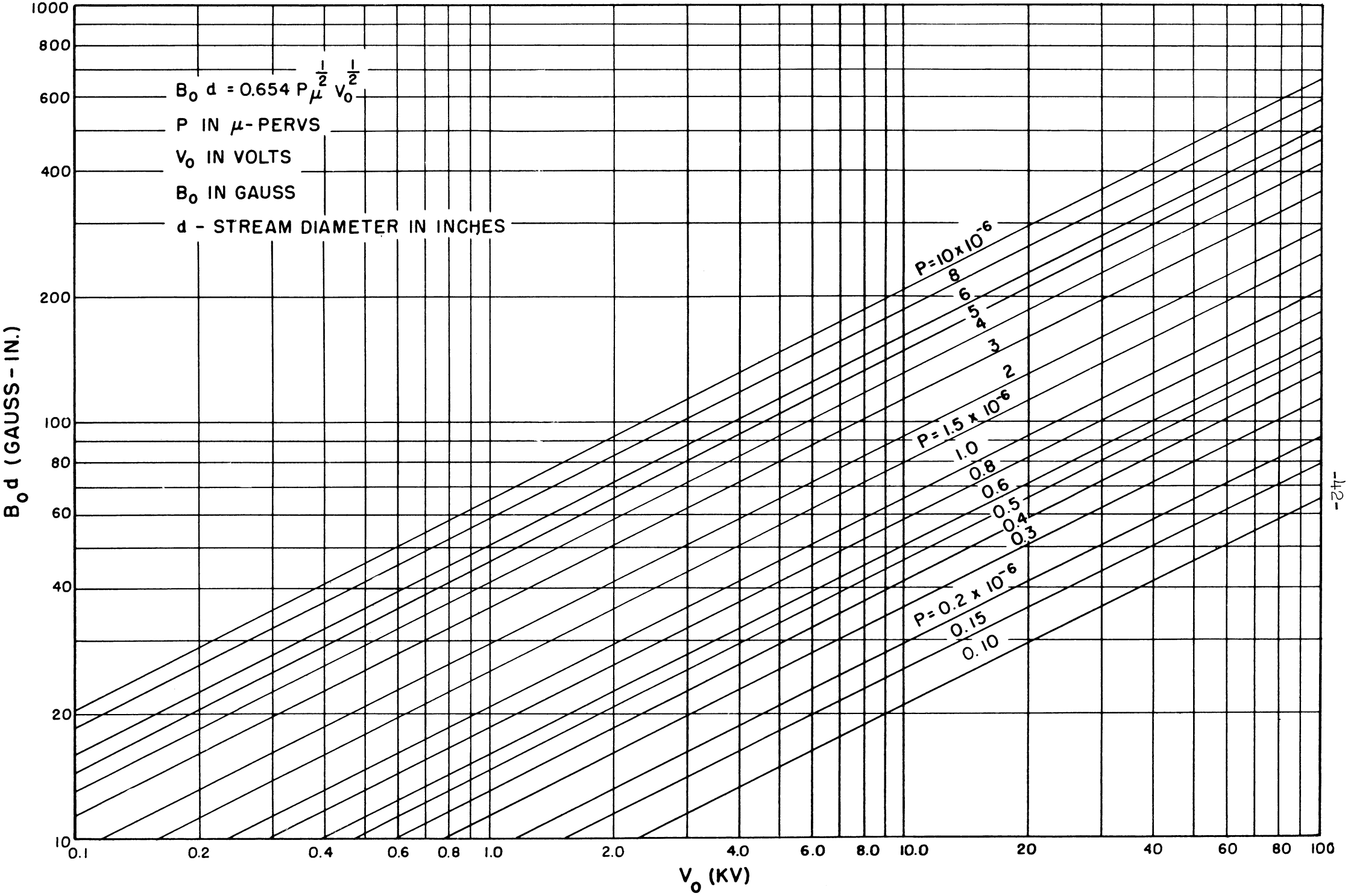
$B_0\ d = 0.654\ P\mu^{\frac{1}{2}}\ V_0^{\frac{1}{2}}$
P IN μ-PERVS
V_0 IN VOLTS
B_0 IN GAUSS
d - STREAM DIAMETER IN INCHES
P=10x10⁻⁶
8
6
5
4
3
2
P=1.5 x 10⁻⁶
1.0
0.8
0.6
0.5
0.4
0.3
P=0.2 x 10⁻⁶
0.15
0.10
$B_0 d$ (GAUSS-IN.)
1000
800
600
400
200
100
80
60
40
20
10
0.1
0.2
0.4
0.6
0.8
1.0
2.0
4.0
6.0
8.0
10.0
20
40
60
80
100
V_0 (KV)

a. Denote the temporary values of the design parameters selected in (2) and (3) above by the subscript 1. If an r-f structure other than the helix is involved then the value of QC used is the value taken from the large-signal curves divided by the QC for a helix tube. Thus for nonhelix structures

$$(QC)_1 = \frac{QC}{\xi} .$$

b. Use $(QC)_1$ to find the perveance correction factor from Fig. 15. Then

$$P_{\mu 1}(1+Cb)^2 = \frac{P_{\mu 1}}{(\text{ordinate of Fig. 15})} .$$

c. Enter the appropriate curve of the type shown in Figs. 13 and 14 with $P_{\mu 1}(1+Cb)^2$ and B_1 to find $(QC)_2$.

d. If $(QC)_2 \neq (QC)_1$, then change to a $P_{\mu 2}(1+Cb)^2$ such that $(QC)_2 = (QC)_1$ for the same B_1. Using $(QC)_2$ determine $P_{\mu 2}$ from Fig. 15.

e. Find I_{O2} and V_{O2} to give P_{O1}.

f. From the appropriate curve of $QC/(1+Cb)$ vs. B, find $(QC)_3/(1+Cb)$ for V_{O2} and C_1.

g. If $(QC)_3/(1+Cb) \neq (QC)_1/(1+Cb)$ then select $(QC)_3/(1+Cb)$ and find $(QC)_3$ using the correction contained in Fig. 10.

h. Find $P_{\mu 3}(1+Cb)^2$ using $(QC)_3$ and B_1. Use Fig. 15 to get $P_{\mu 3}$.

i. Find η_{s2} from the large-signal curves using $(QC)_3$, C_1 nnd B_1.

j. Calculate P_{b2} to give P_O using η_{s2} as the efficiency.

k. Find V_{o3} and I_{o3} using P_{b2} and $P_{\mu 3}$.

l. Compare V_{o3} and V_{o2}; if they differ appreciably determine $(QC)_4$ at V_{o3}.

m. Repeat the above-outlined process until $V_{o3} \cong V_{o2}$. This is usually not necessary after some experience in using the curves is acquired.

If success is not achieved after several iterations, then the values of B and C selected are not consistent with the desired power output. In this case compromises are obviously necessary. Usually the difficulty will be remedied by increasing B, which has the advantage that for a fixed value of a'/b' the value of $\gamma a'$ is increased.

5. The value of y corresponding to the value of b chosen earlier is found from the small-signal solutions. Since the beam voltage has been determined and the center frequency is known, the value of λ_g and hence the value of a', the mean helix radius, can be calculated assuming that the phase velocity of the r-f wave is given by

$$v = v_o \frac{1 + Cb}{1 - Cy} .$$

From this point on the design procedure will be directed toward helix-type tubes. Other r-f structures will require different methods for determining actual structure dimensions.

6. Since a'/b' has been fixed, the beam radius b' is also determined and the stream current density is specified.

7. The value of λ_g found under part 5 and the value of $\gamma a'$ are used to find the helix T.P.I. from Fig. 19.

8. The helix wire diameter is usually chosen to be somewhere between one-quarter and one-half the pitch distance. At s-band it has been shown experimentally and theoretically that there is a broad minimum in the attenuation curve for a ratio of wire diameter to pitch around one-third[14,15].

9. The first estimate of the length of the helix structure in terms of N_g may be found from the large-signal curves where d = 0. The optimum circuit length as a function of the input-signal level is shown in Fig. 24. The input-signal level is referred to CI_oV_o and the saturation level is approximately 5 db above CI_oV_o. The large-signal curves for which $d \neq 0$, shown in Figs. 25 and 26, may be used to estimate the added length in terms of N_g's necessary to recover the gain lost in the attenuator region. These curves not only show the loss in saturation power due to attenuation but also indicate the effect on the saturation power level of the placement of the attenuator.

10. An alternate method for determining the helix length for a given useful gain is to use the small-signal gain equation $G = A + BCN_g$. Since the value of C has previously been determined and A and B may be found from Pierce's small-signal theory, the tube length for a given loss-free small-signal gain may be computed. The large-signal (saturation) gain in db down from the small-signal gain may be found from a large-signal plot of the saturation power output in db down from small signal for the particular values of C, QC and B previously selected. The reduction in saturation level due to large-signal effects is shown in Fig. 27.

FIG. 24

ψ, INPUT-SIGNAL LEVEL IN db BELOW $C I_0 V_0$, VS. TUBE LENGTH AT SATURATION IN UNDISTURBED WAVELENGTHS. b IS ADJUSTED FOR MAXIMUM SATURATION GAIN

($C = 0.1$, $d = 0$, $B = 1$, $a'/b' = 2$)

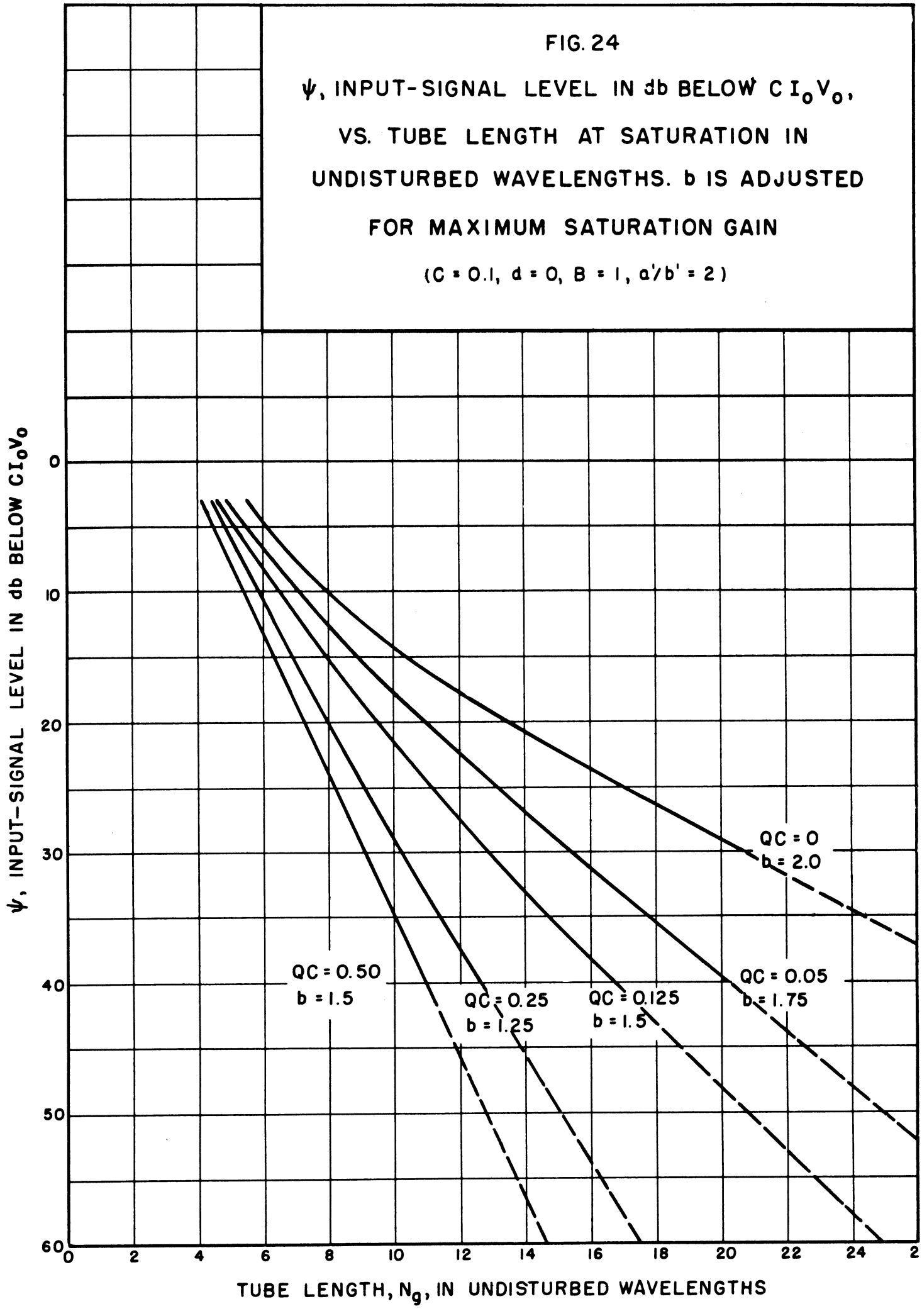

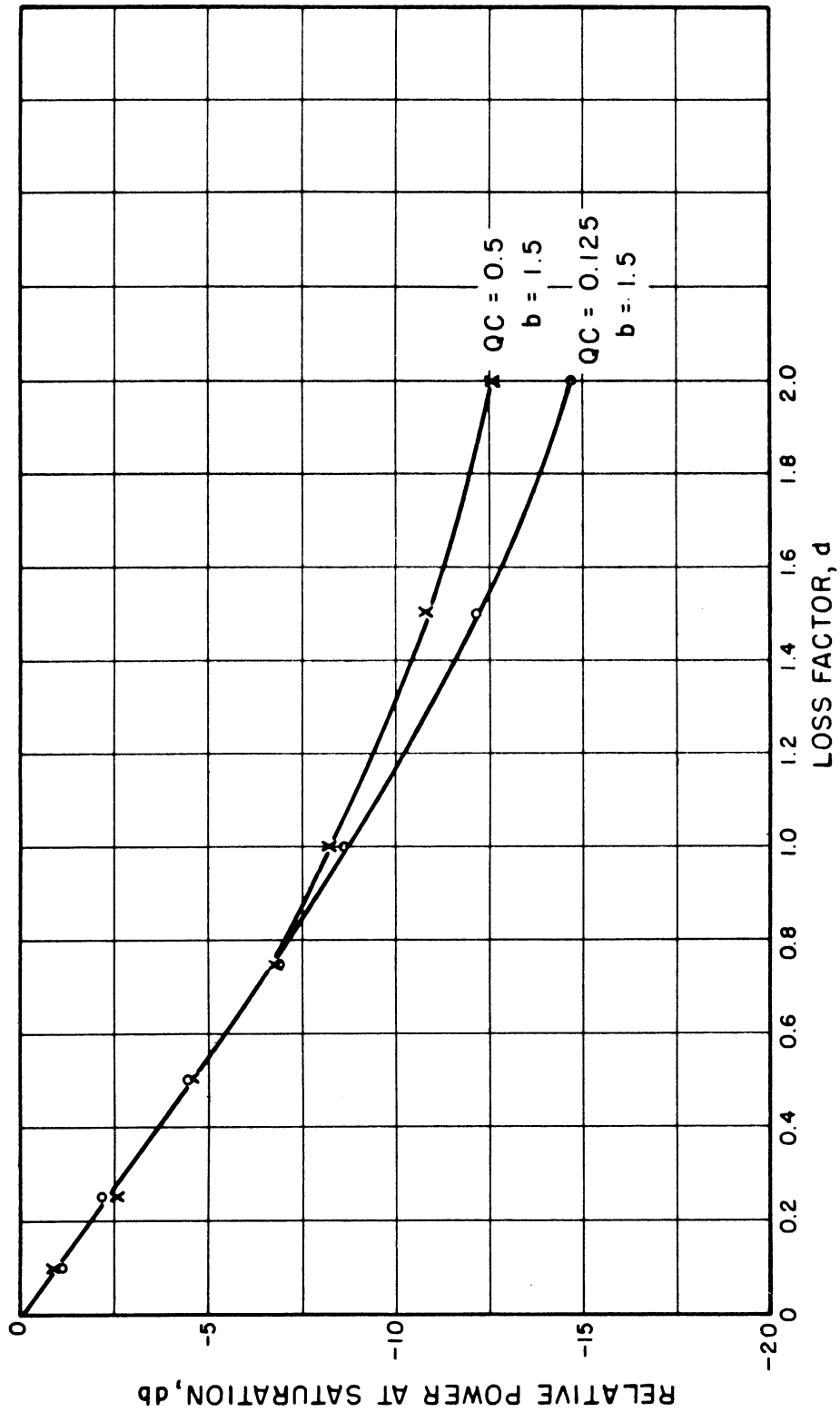

FIG. 25 RELATIVE POWER AT SATURATION VS. LOSS FACTOR WITH SPACE CHARGE AS THE PARAMETER. UNIFORM LOSS STARTING AT CN≈0.3 AND CONTINUING TO SATURATION. (C=0.1, B=1, a'/b' = 2.)

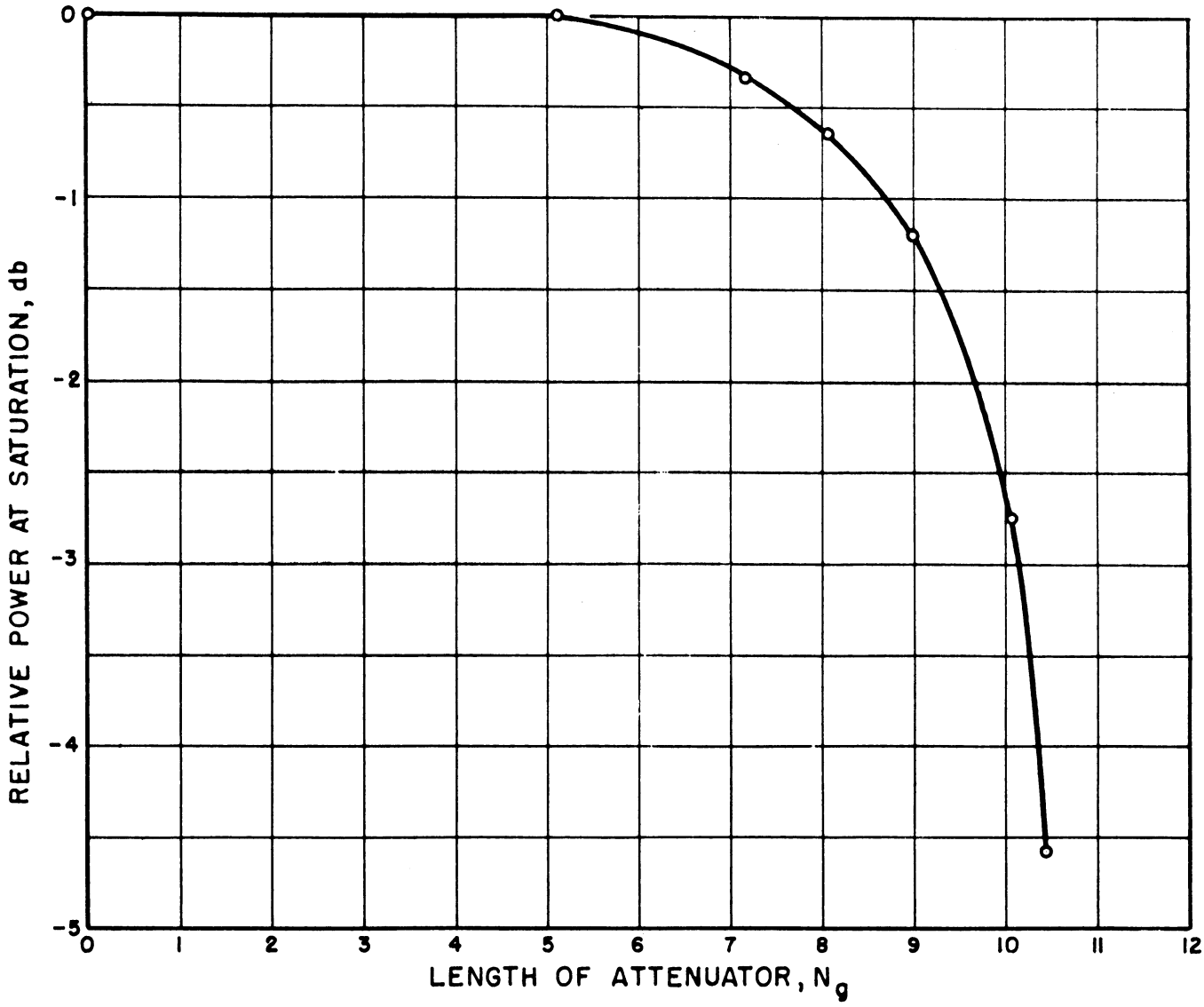

FIG. 26 RELATIVE POWER AT SATURATION VS. ATTENUATOR LENGTH. ATTENUATION STARTS AT CN≈ 0.3. (C = 0.1, QC = 0.125, b = 1.5, B = 1, d = 0.5, a'/b' = 2.)

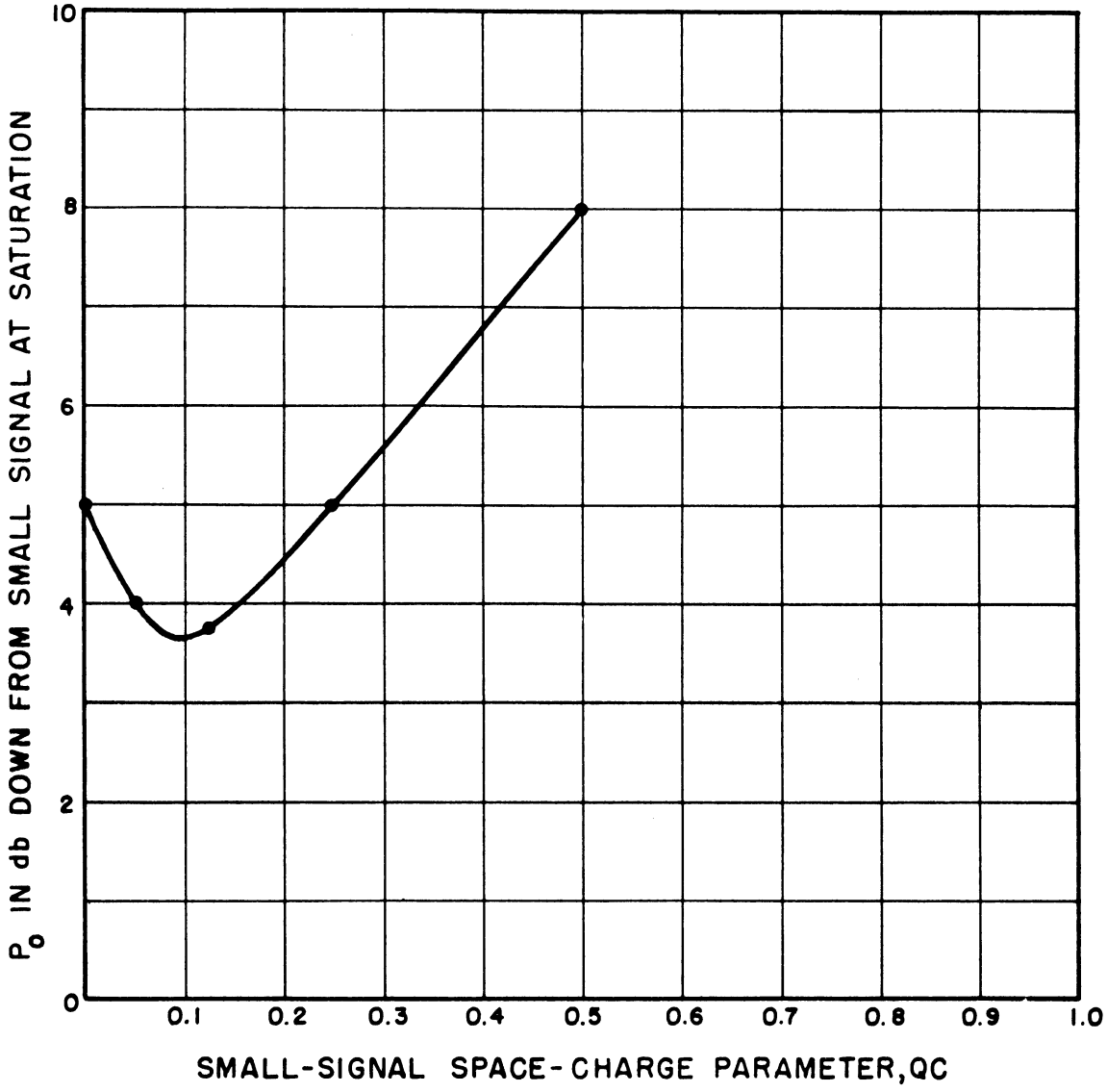

FIG. 27 P_o IN db DOWN FROM SMALL-SIGNAL OUTPUT AT SATURATION VS. SMALL-SIGNAL SPACE-CHARGE PARAMETER. ($C = 0.1$, $d = 0$, $N_g = 5.5$, $B = 1$, $a'/b' = 2.$)

APPLICATION OF THE DESIGN PROCEDURE

In the previous section the general procedure was outlined for the design of either pulsed or cw helix-type traveling-wave amplifiers to operate at as high an efficiency as possible. The procedure is applicable to either low-power or high-power tubes but has greatest value in the design of high-power tubes. The following is an illustration of the use of this procedure in the design of a cw s-band amplifier to operate at high efficiency over a broad frequency range. The design objectives are to achieve at least 200 watts cw output at a 30-db large-signal gain using a wire helix and a solid electron beam. The following steps outline the design of the desired tube.

1. The design is based on P_o = 200 watts and the objective is to obtain as high a saturation efficiency as possible.
2. From the large-signal efficiency curves the following desirable operating parameters are obtained (to give maximum efficiency):

   $C = 0.1$, $QC = 0.125$, $B = 1.0$, $\eta_s = 55\%$, $b = 1.5$, $d = 0$.

   The following parameters are assumed:

   a. Ratio of helix-to-beam radii, $a'/b' = 1.4$.
   b. DLF = 90% for a helix supported in glass by three quartz or sapphire rods.
   c. It is desirable to have $1.5 < \gamma a' < 2.1$ for broadband operation.

   The beam power is then calculated to be

$$P_b = \frac{200}{0.55} = 364 \text{ watts.}$$

3. The beam perveance is assumed to be 1×10^{-6}, which gives the following values of V_o and I_o for P_b = 364 watts:

$V_o = 2650$ volts

$I_o = 137$ ma.

4. The next step is to determine whether the desired operating parameters can be achieved with a helix-type tube. Denote the assumed values by the subscript one.

   a. $(QC)_1 = 0.125$, $C_1 = 0.1$, $B_1 = 1.0$, $V_{o1} = 2650$ volts and $I_{o1} = 137$ ma.

   b. From Fig. 15 for $(QC)_1 = 0.125$, $P_{\mu 1}(1+Cb)^2 = \frac{1}{0.758} = 1.32$.

   c. From Fig. 13 it is found that $(QC)_2 = 0.25 \neq (QC)_1$.

   d. Since $(QC)_2 \neq (QC)_1$ the perveance is changed so that $(QC)_2 = (QC)_1$ for the same B_1. This give $P_{\mu 2}(1+Cb)^2 = 0.625$. Using $(QC)_2$ to determine $P_{\mu 2}$ from Fig. 15 gives

$$P_{\mu 2} = \frac{0.625}{0.758} = 0.825.$$

   e. For $P_{\mu 2} = 0.825$ and $P_b = 364$ watts, $V_{o2} = 2850$, $I_{o2} = 128$ ma.

   f. Using $C_1 = 0.1$ and $V_{o2} = 2850$ and Figs. 5 and 6 gives

$$\frac{(QC)_3}{1 + Cb} = 0.18. \quad \text{Note that } \frac{(QC)_1}{1 + Cb} = 0.11.$$

   g. Since $(QC)_3/(1+Cb) \neq (QC)_1/(1+Cb)$, $(QC)_3/(1+Cb)$ is selected and $(QC)_3$ is found from Fig. 10. $(QC)_3 = 0.202$.

   h. $P_{\mu 3}(1+Cb)^2 = 1.04$ from Fig. 13 using $(QC)_3$ and B_1. Thus $P_{\mu 3} = 1.04(0.781) = 0.811$ from Fig. 15.

   i. From the large-signal efficiency curve shown in Fig. 1, $(QC)_3$, C_1 and B_1 will give an efficiency $\eta_{s2} = 45\%$.

j. Thus $P_{b2} = \frac{200}{0.45} = 444$ gives

$$V_{o3} = 3120 \text{ volts and } I_{o3} = 143 \text{ ma.}$$

k. $V_{o3} = 3120$ volts is not equal to $V_{o2} = 2850$ volts. However, the values of QC do not differ appreciably; hence the process is assumed to be complete.

Thus the final design parameters are:

C = 0.1	V_o = 3120 volts
QC = 0.202	I_o = 143 ma.
B = 1.0	P_μ = 0.811
$\gamma a' = B(a'/b') = 1.4$	b = 1.32.

Throughout the design procedure compromises in QC and hence efficiency were made in order to obtain C = 0.1.

5. The helix voltage corresponding to synchronism is calculated using 1 + Cb = 1.132 from the above material.

$$V(v_o) = \frac{V_o}{(1+Cb)^2} = \frac{3120}{(1.132)^2} = 2430 \text{ and}$$

$$\lambda_g = \frac{5.93 \times 10^5 \, (2430)^{1/2}}{3 \times 10^8} \times 10^2 = 0.977 \text{ cm.}$$

The mean helix radius is then found from

$$\gamma a' = \frac{2\pi a'}{\lambda_g} = 1.4 \ .$$

$$a' = 0.218 \text{ cm. or } 0.0859 \text{ inch.}$$

6. The beam radius $b' = 0.7\ (0.0859) = 0.060$ inch. The beam current density is calculated as

$$J_b = \frac{I_o}{\pi(b')^2} = 1.94 \text{ amps/cm}^2.$$

7. $ka' = \frac{2\pi a'}{\lambda_o} = 0.1375$ and thus $\frac{DLF}{ka'} = \frac{0.90}{0.1375} = 6.55$. From Fig. 19 for $\gamma a' = 1.4$ it is seen that the helix T.P.I. = 18.55.

8. The helix wire diameter is selected to be

$$d_{wire} = \frac{\text{Pitch}}{3} = \frac{1}{3(\text{T.P.I.})} = 0.018 \text{ inch.}$$

No. 24 wire, which is 20.1 mils in diameter, will be used.

9. The helix length for d = 0 is estimated from Fig. 24 to be $N_g = 18$ to obtain a gain of 60 db assuming a 30-db attenuator. Thus there is a gain of 3.33 db/λ_g. The effect of the attenuator in reducing the saturation gain is shown in Figs. 25 and 26. If the 30-db attenuator is made approximately 2 inches long, Fig. 26 indicates there will be no reduction in the saturation level. Additional curves of this type are being calculated for other values of C, QC and d.

The helix length is

$$L = \frac{0.977}{2.54}\ (18) \approx 7 \text{ inches.}$$

CONCLUSIONS

A general design procedure has been developed that facilitates the design of both low-power and high-power large-signal traveling-wave tubes to

operate at high saturation efficiency. The design procedure is directed primarily toward the design of helix-type tubes, but modifications are also presented that facilitate the design of tubes with any type of modified helix structure or with any of the varied forms of periodically loaded waveguides. The procedure permits the rapid design of a tube and has been found to give very satisfactory results at varied frequencies.

ACKNOWLEDGMENTS

The authors wish to express appreciation to their associates for valuable suggestions during the course of the work and in particular acknowledge the aid of Messrs. Masnari, Ohtomo, Pua, and Wen in calculating the design curves.

LIST OF SYMBOLS

a'	mean helix radius
b	injection velocity parameter
$B = \beta b'$	space-charge range parameter
b'	stream radius
c	velocity of light
C	gain parameter
$F = F_1 F_2$	helix-impedance reduction factor
G	impedance gain factor
I_o	d-c stream current
K_d	impedance of a modified helix or periodically loaded waveguide structure
K_s	sheath helix impedance
P	stream perveance
P_o	power output
P_μ	stream micropervs
$P_{\mu d}$	stream micropervs for tubes with modified helix or periodically loaded waveguide structures
$P_{\mu h}$	stream micropervs for a helix tube
QC	space-charge parameter
$(QC)_d$	space-charge parameter for tubes with modified helix or periodically loaded waveguide structures
$(QC)_h$	space-charge parameter for a helix tube
R	plasma frequency reduction factor
R_d	plasma frequency reduction factor for modified helix and periodically loaded waveguide structures

LIST OF SYMBOLS
(Continued)

R_h	plasma frequency reduction factor for a helix tube
u_o	d-c stream velocity
v_o	undisturbed circuit phase velocity
V_o	d-c stream voltage
y	small-signal phase constant of the r-f wave
β	wave phase constant
β_e	stream phase constant
$\beta_o = k_i = k$	free-space phase constant
$\gamma = (\beta^2-\beta_o^2)^{1/2}$	radial propagation constant
$\eta = e/m$	charge-to-mass ratio for the electron
η_s	saturation efficiency, percent
κ	perveance correction factor
ξ, ν	space-charge parameter correction factors
ψ	helix pitch angle; also input-signal level relative to CI_oV_o
ω	radian frequency
ω_p	radian plasma frequency
$\omega_q = R\omega_p$	effective radian plasma frequency

LIST OF REFERENCES

1. Rowe, J.E., "A Large-Signal Analysis of the Traveling-Wave Amplifier: Theory and General Results", Trans. PGED-IRE, Vol. ED-3, pp. 39-57; January, 1956.

2. Rowe, J.E., "Design Information on Large-Signal Traveling-Wave Amplifiers", Proc. IRE, Vol. 44, No. 2, pp. 200-211; February, 1956.

3. Rowe, J.E., "Large-Signal Traveling-Wave Amplifiers", Tech. Rpt. No. 20, Electrical Engineering Department, Electron Tube Laboratory, The University of Michigan; December, 1956.

4. Cutler, C.C., "The Nature of Power Saturation in Traveling-Wave Tubes", BSTJ, Vol. 35, No. 4, pp. 841-876; July, 1956.

5. Caldwell, J.J., Hoch, O.L., "Large Signal Behavior of High Power Traveling-Wave Amplifiers", Trans. PGED-IRE, No. 1, pp. 6-18; January, 1956.

6. Tien, P.K., "A Large Signal Theory of Traveling-Wave Amplifiers, Including Effects of Space Charge and Finite Coupling between Beam and Circuit", BSTJ, Vol. 35, No. 2, pp. 349-374; March, 1956.

7. Fletcher, R.C., "Helix Parameters Used in Traveling-Wave-Tube Theory", Proc. IRE, Vol. 38, No. 4, pp. 413-417; April, 1950.

8. Tien, P.K., "Traveling-Wave Tube Helix Impedance", Proc. IRE, Vol. 41, No. 11, pp. 1617-1624; November, 1953.

9. These data were obtained from the quartic determinantal equation by Hill's method.

10. Tien, P.K., op. cit.

11. Birdsall, C.K., Everhart, T.E., "Modified Contra-Wound Helix Circuits for High-Power Traveling-Wave Tubes", Trans. PGED-IRE, No. 4, pp. 190-205; October, 1956.

12. Pierce, J.R., Theory and Design of Electron Beams, Van Nostrand Company, New York, 1949; Chap. 9.

13. Brewer, G.R., "Some Effects of Magnetic Field Strength on Space-Charge-Wave Propagation", Proc. IRE, Vol. 44, No. 71, pp. 896-903; July, 1956.

14. Olson, A.B., Peter, R.W., Ruetz, J.A., "Attenuation of Wire Helices in Dielectric Supports", RCA Review, Vol. 13, pp. 558-573; December, 1952.

15. Chu, C.M., "Effect of Conductor Size and Shape on the Propagation of Waves in Helical Waveguides", Engineering Research Institute Report No. 2144-193J, The University of Michigan, Ann Arbor, Michigan; 1957.

DISTRIBUTION LIST

No. Copies	Agency
3	Commander, Rome Air Development Center, ATTN: RCERRT, Griffiss Air Force Base, New York
1	Commander, Rome Air Development Center, ATTN: RCSSTW, Griffiss Air Force Base, New York
1	Commander, Rome Air Development Center, ATTN: RCSSLD, Griffiss Air Force Base, New York
12	Armed Services Technical Information Agency, Documents Service Center, Arlington Hall Station, Arlington 12, Virginia
1	Commander, Air Force Cambridge Research Center, ATTN: CRQSL-1, Laurence G. Hanscom Field, Bedford, Massachusetts
1	Director, Air University Library, ATTN: AUL-7736, Maxwell Air Force Base, Alabama
2	Commander, Wright Air Development Center, ATTN: WCOSI-3, Wright-Patterson Air Force Base, Ohio
2	Commander, Wright Air Development Center, ATTN: WCOSR, Wright-Patterson Air Force Base, Ohio
1	Air Force Field Representative, Naval Research Laboratory, ATTN: Code 1010, Washington 25, D. C.
1	Chief, Naval Research Laboratory, ATTN: Code 2021, Washington 25, D. C.
1	Chief, Bureau of Ships, ATTN: Code 312, Washington 25, D. C.
1	Commanding Officer, Signal Corps Engineering Laboratories, ATTN: Technical Reports Library, Fort Monmouth, New Jersey
1	Chief, Research and Development Office of the Chief Signal Officer, Washington 25, D. C.
1	Commander, Air Research and Development Command, ATTN: RDTDF, Andrews Air Force Base, Washington 25, D. C.
1	Commander, Air Research and Development Command, ATTN: RDTC, Andrews Air Force Base, Washington 25, D. C.
1	Director, Evans Signal Laboratory, Belmar, New Jersey, ATTN: Mrs. Betty Kennett, Report Distribution Unit, Electron Devices Division
1	Chief, European Office, Air Research and Development, Shell Building, 60 Rut Cantersteen, Brussels, Belgium

DISTRIBUTION LIST
(Continued)

No. Copies	Agency
1	Secretariat, Advisory Group on Electron Tubes, 346 Broadway, New York 13, New York
1	California Institute of Technology, Department of Electrical Engineering, Pasadena, California, ATTN: Prof. L. M. Field
1	University of California, Electrical Engineering Department, Berkeley 4, California, ATTN: Prof. J. R. Whinnery
1	University of Colorado, Department of Electrical Engineering, Boulder, Colorado, ATTN: Prof. W. G. Worcester
1	Cornell University, Department of Electrical Engineering, Ithaca, New York, ATTN: C. Dalman
1	General Electric Company, Electron Tube Division of Research Laboratory, The Knolls, Schenectady, New York, ATTN: Dr. E. D. McArthur
1	General Electric Microwave Laboratory, 601 California Avenue, Palo Alto, California, ATTN: Technical Library
1	Huggins Laboratories, 711 Hamilton Avenue, Menlo Park, California, ATTN: L. A. Roberts
1	Hughes Aircraft Company, Electron Tube Laboratory, Culver City, California, ATTN: J. T. Milek
1	Varian Associates, 611 Hansen Way, Palo Alto, California, ATTN: Technical Library
1	Philips Research Laboratories, Irvington on the Hudson, New York, ATTN: Dr. Bernard Arfin
1	Columbia University Radiation Laboratory, 538 West 120th Street, New York 27, New York, ATTN: Technical Library
1	University of Illinois, Department of Electrical Engineering, Electron Tube Section, Urbana, Illinois
1	University of Florida, Department of Electrical Engineering, Gainsville Florida
1	John Hopkins University, Radiation Laboratory, Baltimore 2, Maryland, ATTN: Dr. D. D. King
1	Sperry Rand Corporation, Sperry Electron Tube Division, Gainsville, Florida, ATTN: Technical Library

DISTRIBUTION LIST
(Continued)

No. Copies	Agency
1	Stanford University, Microwave Laboratory, Stanford, California, ATTN: Dr. M. Chodorow
1	Stanford University, Stanford Electronics Laboratories, Stanford, California, ATTN: Dr. D. A. Watkins
1	Raytheon Manufacturing Company, Microwave Power Tube Division, Waltham, Massachusetts, ATTN: Technical Library
1	Federal Telecommunications Laboratories, Inc., 500 Washington Avenue, Nutley, New Jersey, ATTN: Technical Library, Electron Tube Laboratory
1	RCA Laboratories, Electronics Research Laboratory, Princeton, New Jersey, ATTN: Dr. E. H. Herold
1	Eitel-McCullough, Inc., San Bruno, California, ATTN: Mr. Donald Priest
1	Litton Industries, 960 Industrial Road, San Carlos, California, ATTN: Dr. Norman Moore
1	Massachusetts Institute of Technology, Research Laboratory of Electronics, Cambridge 39, Massachusetts, ATTN: Documents Library
1	Sperry Gyroscope Company, Great Neck, New York, ATTN: Engineering Library
1	Polytechnic Institute of Brooklyn, Microwave Research Institute, Brooklyn, New York, ATTN: Technical Library
1	Harvard University, Cruft Laboratory, Cambridge, Massachusetts, ATTN: Technical Library
1	Sylvania Microwave Tube Laboratory, 500 Evelyn Avenue, Mountain View, California, ATTN: Dr. D. Goodman
1	Sylvania Electric Products, Inc., Physics Laboratory, Bayside, New York, ATTN: Dr. R. G. E. Hutter
1	Bell Telephone Laboratories, Inc., Murray Hill Laboratory, Murray Hill, New Jersey, ATTN: Dr. J. R. Pierce
1	University of Washington, Department of Electrical Engineering, Seattle 5, Washington, ATTN: A. E. Harrison
1	Massachusetts Institute of Technology, Lincoln Laboratory, Lexington 73, Massachusetts, ATTN: Mr. Robert Butman